

The origin and depositional architecture of Paleogene quartz-glaucanite sands in the Lubartów area, eastern Poland

Krzysztof CZURYŁOWICZ^{1, 2, *}, Anna LEJZEROWICZ^{1, 3}, Sebastian KOWALCZYK¹
and Anna WYSOCKA¹

¹ Faculty of Geology, University of Warsaw, wirki i Wigury 93, 02-089 Warszawa, Poland

² Polish Geological Institute-National Research Institute, Rakowiecka 4, 00-975 Warszawa, Poland

³ Faculty of Civil Engineering, Warsaw University of Technology, Armii Ludowej 16, 00-637 Warszawa, Poland



Czuryłowicz K., Lejzerowicz A., Kowalczyk S. and Wysocka A. (2014) The origin and depositional architecture of Paleogene quartz-glaucanite sands in the Lubartów area, eastern Poland. *Geological Quarterly*, **58** (1): 125–144, doi: 10.7306/gq.1137

The study uses quantitative methods to analyse the latest Bartonian to Early Rupelian sedimentary succession at the SE outskirts of the Polish Lowland Paleogene Basin, in the back-bulge zone of the Carpathian orogenobulge. The vertical lithotype proportion diagrams from a large number of well logs are compiled to reveal the area's sequence stratigraphy. Six sequences are recognized and correlated with 3rd-order eustatic sea level cycles. The basal sequence of type 1 is overlain by three sequences of type 2 and followed by a fifth sequence of type 1, whose depositional forced-regressive and lowstand systems tracts brought the main volume of quartz-glaucanite sand to the study area. The study focuses further on the deposits of this fifth sequence, exposed and surveyed with GPR in the Nowodwór-Piaski sand pit. Their sedimentary facies analysis reveals the local spatial pattern of a wave-dominated and tidally-influenced sedimentation, supporting the earlier notions of a southern palaeoshoreline and a tectonically-controlled sedimentation. The analysis, aided by multidimensional GPR survey, indicates syndepositional development of a tectonic graben filled laterally by fault scarp-attached large sand bars and an axial action of tidal ebb currents. The bars were formed of shore-derived sand swept by littoral waves from the graben footwall areas. As the graben's tectonic activity ceased, it became buried by the lowstand regressive sands overlain by gravelly foreshore deposits, most of which were later removed by the Pleistocene glacial erosion. A 3D model of the deposits in the Nowodwór-Piaski area is constructed on the basis of outcrop and GPR data with the use of multiple-point statistical methodology to depict the internal architecture, heterogeneity and spatial relationships of main sedimentary facies. The model can serve as a guide for the future exploration and exploitation of the quartz-glaucanite sands in the area and as instructive example of how a petroleum reservoir model of a complex sedimentary succession can be constructed with the use of modern statistical methods.

Key words: littoral facies, syndepositional tectonics, extensional graben, sequence stratigraphy, ground-penetrating radar, 3D modelling.

INTRODUCTION

The present paper reports on the preliminary results of a research project aimed to determine the origin and mineral resource potential of the Paleogene amber-bearing deposits in the northern part of the Lublin district, eastern Poland. These quartz-glaucanite sands occur in an area of 46 km² near Lubartów (Fig. 1) and have long been subject to open-pit mining before attracting detailed geological studies.

On the basis of drilling cores, the quartz-glaucanite sands were originally considered to be a single massive lithosome.

Morawski (1960) conducted a comparative statistical study of sedimentary and mineralogical data from the upper gravelly sands in outcrops in the Lublin region. He ascribed an Oligocene age to the sands and attributed their origin to an Early Oligocene marine transgression that entered the area from the north. Subsequent studies of these deposits were related to the programme of a detailed geological mapping of Poland in the mid-1980s, which allowed determining of the areal extent and full mineral composition of the sands (Łozińska-Stępień et al., 1985). A prospecting drilling project conducted in the northern part of the Lublin region gave a complete stratigraphic profile of the deposits near Lubartów (Kasiński et al., 1997; Kasiński and Tołkanowicz, 1999). Numerous occurrences of amber were documented in glauconitic sandy silts underlying the quartz-glaucanite sands (Woźny, 1966a, b; Kosmowska-Ceranowicz et al., 1990) and several detailed mineralogical studies have recently been conducted (Franus et al., 2004; Franus and Latosińska, 2009; Franus, 2010). Regional lithostratigraphic correlations (Morawski, 1960) combined with biostratigraphic

* Corresponding author, e-mail: krzysztof.czurylowicz@pgi.gov.pl

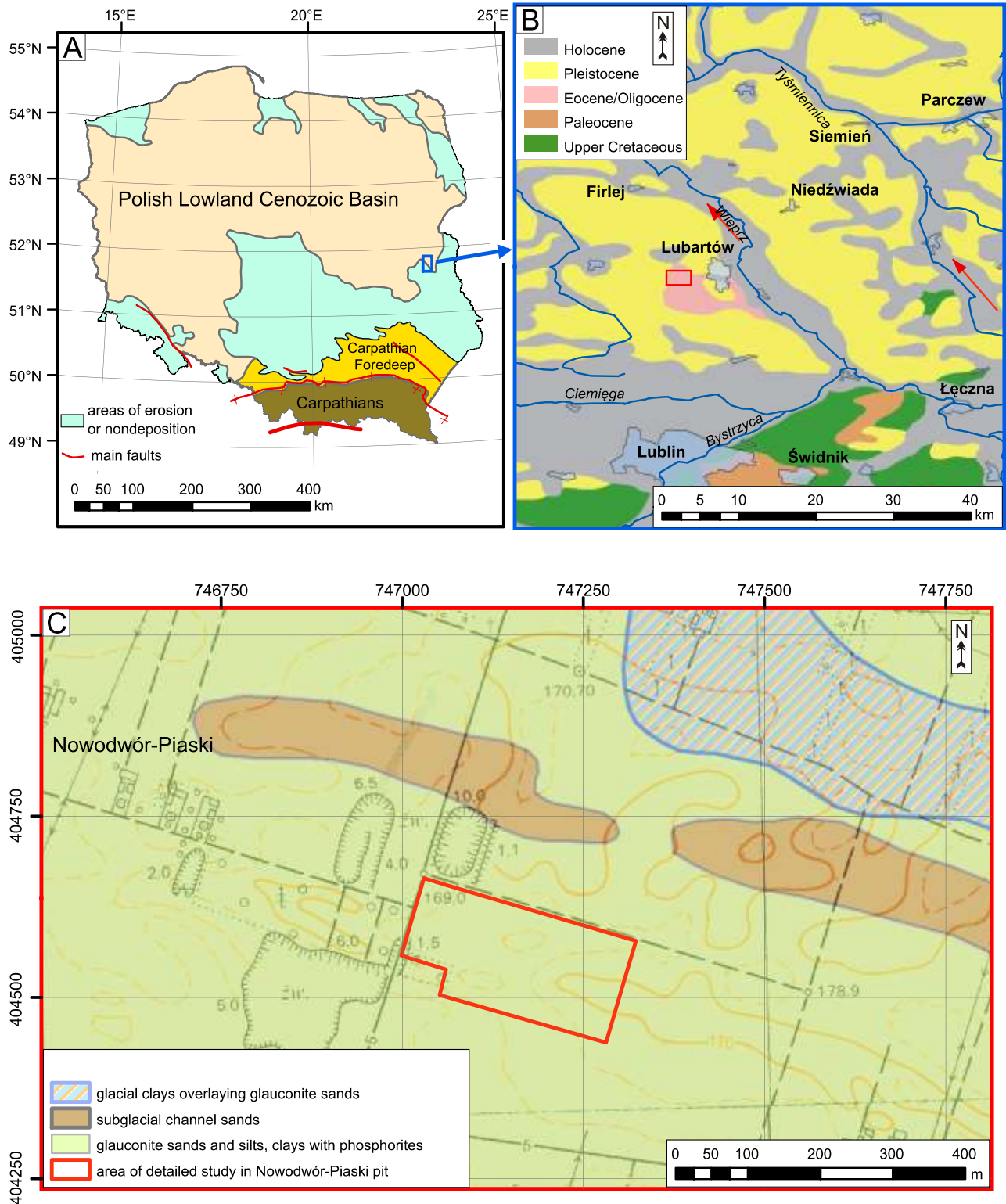


Fig. 1. Location of the study area

A – simplified sub-Quaternary geological map of Poland showing the present-day extent of Paleogene and Neogene deposits (modified from [Asch, 2005](#)); **B** – discussed area shown as a portion of the Geological map of Poland in 1:200,000 scale, with the local river drainage system, main towns and location of the study area (red frame); **C** – topographic and detailed geological map of the study area in 1:50,000 scale ([Łozi ska-St pie et al., 1985](#)), showing the Nowodwór-Piaski open pit and the area of detailed sedimentological and GPR surveys (red frame)

dates (Kasi ski and Tołkanowicz, 1999; Olszewska-Nejbert and Barski, 2007) from our study area have indicated an Eocene-Oligocene time span of the deposits. Newer excavations have also allowed sedimentological studies and spatial analysis of sedimentary facies, as preliminarily reported in this paper.

The aim of the present study was to reconstruct the spatial facies architecture of quartz-glaucanite sands exposed in the Nowodwór-Piaski pit near Lubartów (Fig. 1B, C) and to interpret their depositional environment. The open pit is now at the last stage of exploitation, but fieldwork was conducted in 2009–2012 during the active mining. It was thus possible to produce a comprehensive cartographic documentation of the excavated deposits, to recognize sedimentary structures, main facies and bounding surfaces, to collect palaeocurrent measurements and to conduct GPR surveys. The methodology employed has combined conventional sedimentology, GPR survey and 3D geological mapping techniques. Modern geostatistical tools, such as vertical lithotype proportion diagrams (Buchem et al., 2000; Ravenne, 2002a, b) and multiple-point statistics (Strebelle and Zhang, 2005), have been used to quantify the spatial distribution of sedimentary facies, to recognize transgressive-regressive sequences and to verify stratigraphic correlations (Ravenne et al., 2002). The data allow reconstruction of the depositional architecture of sedimentary facies and shed new light on the origin of the Paleogene quartz-glaucanite sands in this part of the Polish Lowland Basin, indicating a littoral nearshore environment affected by syndepositional fault tectonics.

GEOLOGICAL SETTING

The study area is located in the tectonic province of the East European Platform, at the southeastern extremity of the Polish Lowland Cenozoic Basin (Fig. 1A). The study focuses on an area west of the town of Lubartów (Fig. 1B), where excavations of the Nowodwór-Piaski open pit afford large outcrops of the Paleogene quartz-glaucanite sands (Fig. 1C).

The Paleogene sands overlie directly Mesozoic marls and limestones, with a basal transgressive silty horizon bearing phosphate concretions (Łozi ska-St pie et al., 1985; Kasi ski et al., 1997; Kasi ski and Tołkanowicz, 1999), and are patchily covered by Pleistocene glacial deposits (Fig. 1C). The sub-Paleogene bedrock surface shows an overall lowering towards the north (Fig. 2), with a regional-scale palaeotopographic relief of up to ~76 m and southward onlap by Eocene to Oligocene deposits (Fig. 3). The bulk stratigraphy can be revealed only by regional compilations (such as the synthetic profile in Fig. 3, left), as no drilling core shows the entire succession in a single continuous vertical profile (Kasi ski et al., 1997).

The basal surface shows also significant local-scale relief, particularly in the Siemie area to the north (Fig. 1B), where isolated occurrences of relatively thick Upper Eocene are preserved in palaeotopographic depressions (Kosmowska-Ceranowicz et al., 1990; Piwocki, 2002). A similar local anomaly is indicated by the belt of relatively thick uppermost Eocene-Lower Oligocene sands in the present study area (profile I in Fig. 3). At least some of these palaeotopographic depressions could be related to syndepositional normal faulting (Łozi ska-St pie et al., 1985; Kasi ski et al., 1997), as the Variscan compressional deformation in this part of the East European Platform (Henkiel, 1983) was followed by an extensional reacti-

vation of basement faults and brittle deformation of the Cretaceous bedrock (Krzywiec, 2007).

An exploration well drilled near the study area in the Nowodwór-Piaski pit showed the local thickness of Paleogene deposits to be ~18 m. Only the sand-rich uppermost part of this succession, ~9-m-thick, has been exposed by the pit excavations (Fig. 3B). The lowest exposed deposits, 4-m-thick, are glauconitic sandy silts (Fig. 3A, C) intercalated with phosphate-bearing black silts. Their content of foraminifers, calcareous nannoplankton and dinocysts indicates an Eocene age of these deposits and allows them to be ascribed to the Siemie Formation (Kasi ski et al., 1997; Piwocki, 2002). The overlying deposits, 14-m-thick, are medium- to coarse-grained quartz-glaucanite sands, gravelly near the top (Kasi ski et al., 1997). Following Morawski (1960), the sands are considered to be of an Oligocene age.

The origin of the marine quartz-glaucanite sands near Lubartów has remained unclear and controversial. The area location suggests sand deposition in a southeastern marginal zone of the Polish Lowland Basin (Fig. 1A), although no lateral transition to either coastal deposits to the SE or open-marine shelf deposits to the NW has been recognized. Morawski (1960) had focused on the upper gravelly deposits and interpreted them as a transgressive lag emplaced erosionally over a sandy lower shoreface. However, it remained unclear as to how a marine transgression could cover the lower shoreface zone with thick sandy gravel instead of drowning it and covering with silty offshore-transition deposits. Kasi ski and Tołkanowicz (1999) paid more attention to the underlying sands and attributed them to a barrier-island system. However, there are no associated lagoonal deposits and also the spatial architecture of large foresets in these sands (discussed in the present paper) is incompatible with a coastal barrier model.

METHODOLOGY

A multi-scale 3D approach combining various types of geological data (Caumon et al., 2009) has been employed in the present study to reconstruct spatial stratigraphic architecture of the sedimentary succession. The recognition of facies and their relationships on a local outcrop scale gives highly fragmentary insights, and it is only the integration of a wider range of data that can provide an objective regional reconstruction. For this purpose, the conventional sedimentological methodology of outcrop studies (Collinson and Thompson, 1982; Tucker, 2003) has been combined with a selected range of other methods, which are described briefly below. Sequence stratigraphic nomenclature is after Catuneanu (2006) and Helland-Hansen (2009).

THE VLPD PLOTS

The vertical lithotype proportion diagram (VLPD), known also as vertical proportion curve, is a robust quantitative tool that was originally designed to account for nonstationarity in stochastic models and to analyse 1D distribution and sequential organization of facies at the scale of a stratigraphic formation or sedimentary basin, thereby revealing spatial-genetic relationships of facies in the depositional system. The VLPD plots depict upward changes in the proportion of lithotypes computed for predefined thickness intervals of individual pro-

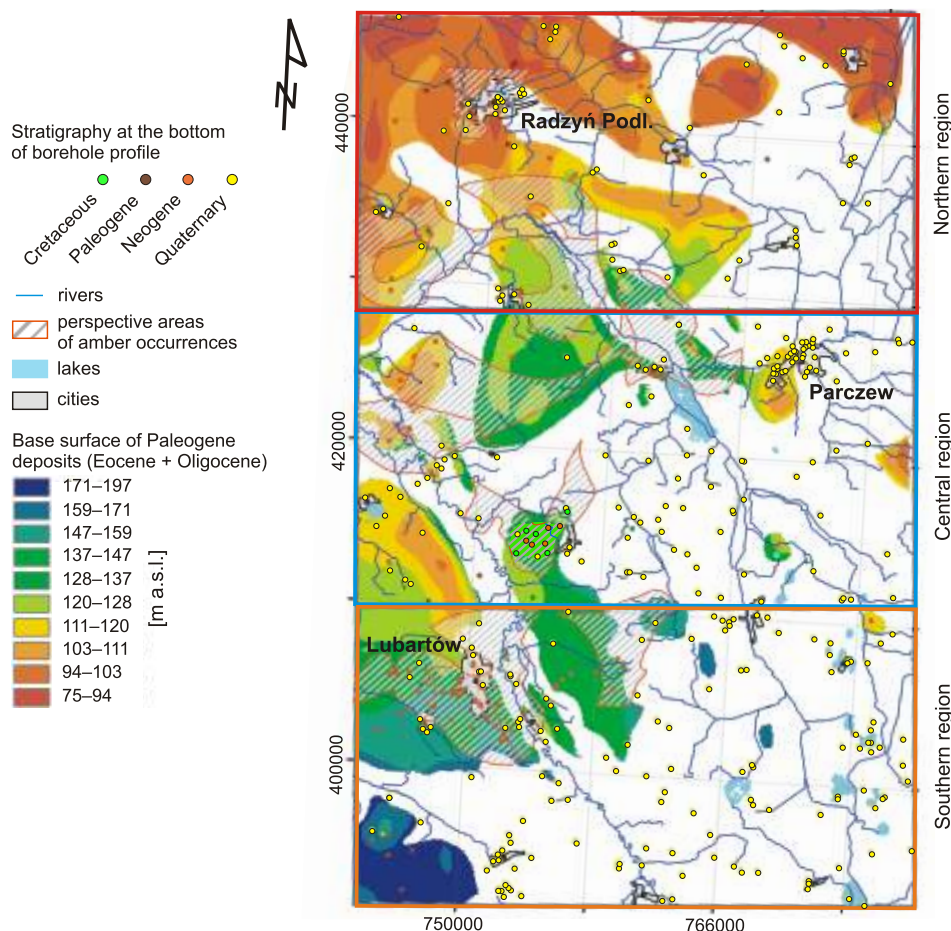


Fig. 2. Map showing the location of boreholes from which data have been used to create a vertical lithotype proportion diagram (VLPD) for the whole area, covering the sheets

Note the general lowering of the base-Paleogene surface towards the north; the three arbitrary regions in the map correspond to the VLPDs shown in Figure 3

files (Buchem et al., 2000; Ravenne et al., 2002; Ravenne, 2002a). The vertical changes in lithotype proportion reveal sedimentary cycles and thus allow distinction of systems tracts and stratigraphic sequences (Fig. 3), which are then compared with the global record (Fig. 4) to recognize eustatic and local tectonic influences. The VLPDs allow also to assess the relative role of particular sedimentary environments and depositional processes in probabilistic (percentage) terms and to recognize changes in the basin accommodation space (Ravenne et al., 2002; Purkis et al., 2012). The usefulness of this tool was demonstrated for the recognition of chronostratigraphic markers (Volpi et al., 1997) and visualization of spatial facies changes within depositional sequences (Ravenne, 2002b; Armstrong et al., 2011).

To create such diagrams for the study area, the numerous lithological profiles of boreholes (Fig. 5) from various databases of the National Geological Archive were used, including the Central Geological Database (CBDG) and Central Hydrogeological Data (HYDRO) Bank, along with published data (Kosmowska-Ceranowicz et al., 1990) and unpublished field documentations (Parecki and Bujakowska, 2004). Lithotypes were distinguished on the basis of sediment grain size and

lithological well-log descriptions. The available biostratigraphic data from Eocene deposits (Wo ny, 1966a, b; Mojski et al., 1966; Uberna and Odrzywolska-Bie kowa, 1977; Kosmowska-Ceranowicz et al., 1990; Kasi ski et al., 1997; Kosmowska-Ceranowicz and Leciejewicz, 1995; Piwocki, 2002) were also incorporated in the diagrams. The primary task was to create a spatial geological model of the post-Cretaceous sedimentary succession (Fig. 5) and to recognize stratigraphic horizons that might serve as reference surfaces in architectural and exploration studies.

The choice of an appropriate reference level for the geometry of sedimentary unit is crucial for the calculated result of the vertical succession of lithotype proportions (Armstrong et al., 2011) and for the recognition and interpretation of systems tracts (transgressive vs. normal- or forced-regressive). These limitations of vertical proportion curve have been taken into account in the present study using a single reference level. For example, the interpretation of silt-rich peaks has been verified on the basis of the available core facies and outcrop observations, which simultaneously allowed verifying whether the chosen reference level is appropriate for the studied depositional system (Armstrong et al., 2011).

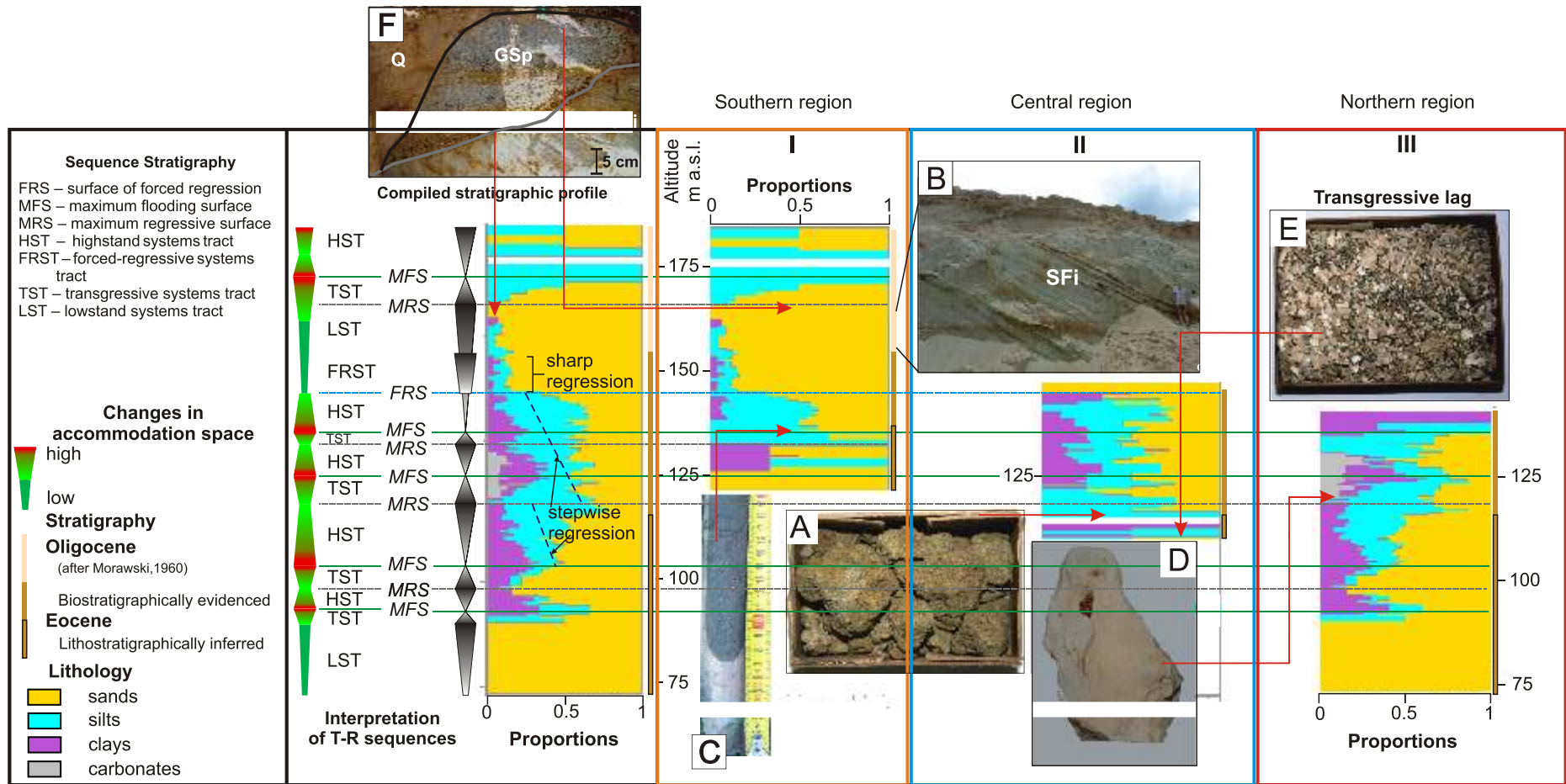


Fig. 3. Vertical lithotype proportion diagrams I-III of Paleogene deposits from separate wells in the three map regions in Figure 2 and their compilation with a sequence stratigraphic interpretation (left)

The inserted photographs show the corresponding main lithotypes: **A** – glauconite sandy silts of the Siemie Formation; **B** – quartz-glaucanite sands in Nowodwór-Piaski pit; **C** – glauconite sandy silts in a core from the vicinity of Ostrów Lubelski; **D** – gaize with fauna shells and amber; **E** – quartz-glaucanite sands with fragments of fauna shells (transgressive lag); **F** – gravelly sand occurring in uppermost part of Nowodwór-Piaski pit; the compiled VLPD indicates that the Paleogene sedimentation commenced with a marine transgression in the northern part of the study area and subsequently extended further to the south

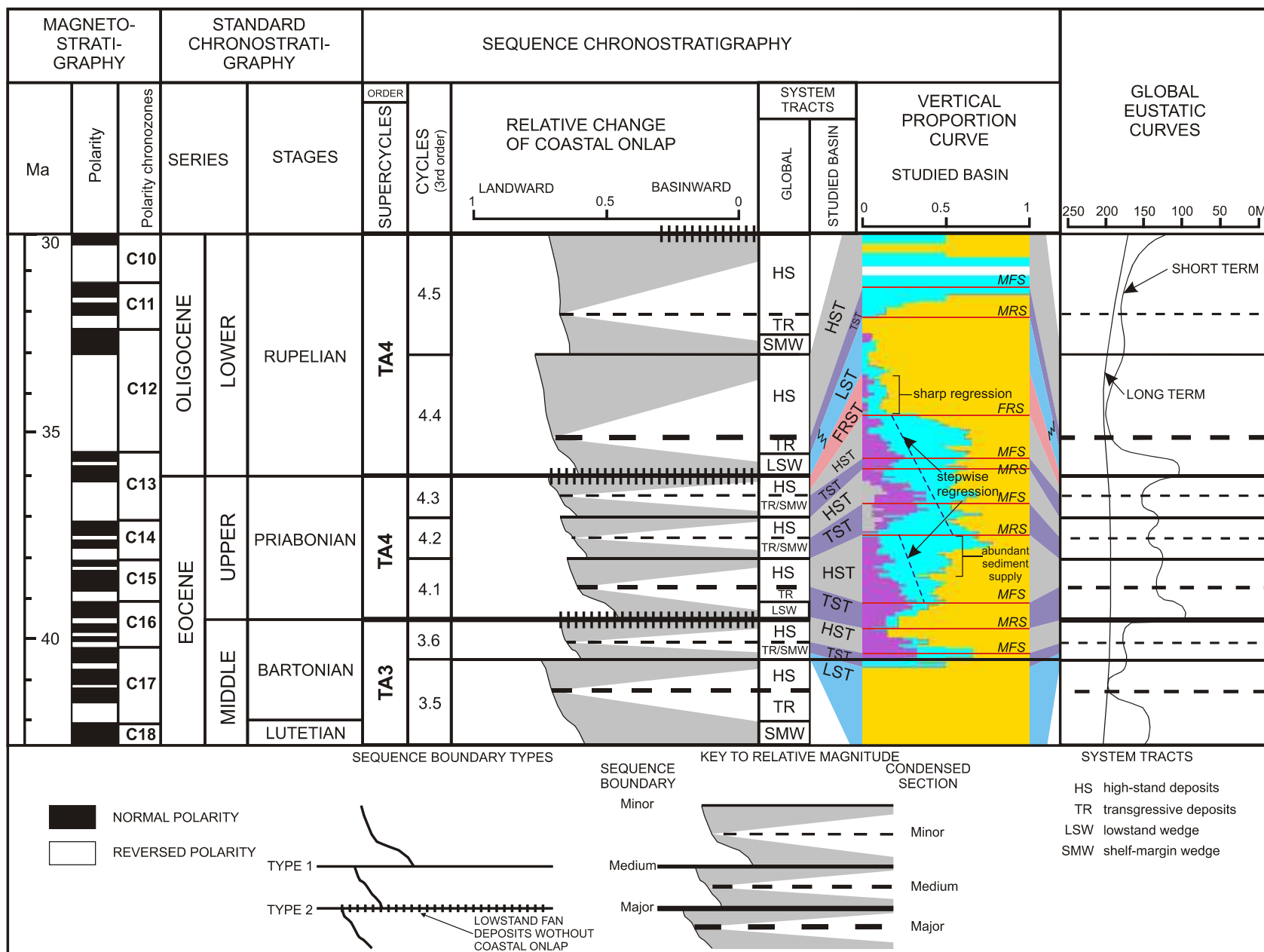


Fig. 4. Correlation of the systems tracts in the studied basin (Fig. 3) with the Middle Eocene to Early Oligocene eustatic pattern of sea level changes (modified from Haq et al., 1987)

For other explanations see Figure 3

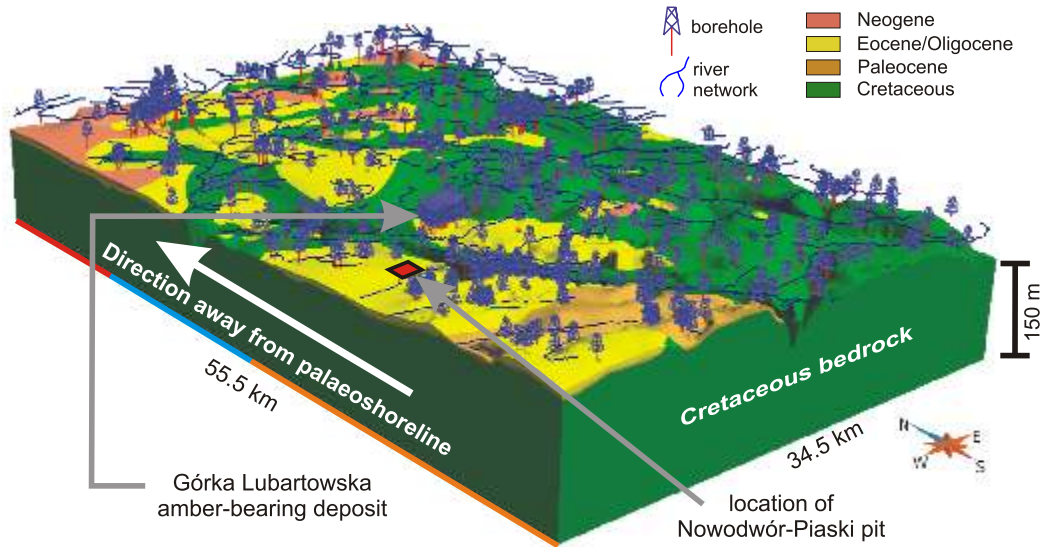


Fig. 5. Spatial stratigraphic model for the study area (Fig. 2) constructed with *Paradigm GOCAD* software

Quaternary cover not included; based on borehole profiles from various databases of the Polish Geological Institute-National Research Institute and other sources (for references, see text)

FIELDWORK AND GPR SURVEY

Fieldwork included collection of sedimentological data for palaeoenvironment reconstruction, such as recognition of sedimentary structures, palaeocurrent measurements, sediment sampling for grain-size analysis and distinction of sedimentary facies (Fig. 6). Both 2D and pseudo-3D ground-penetrating radar (GPR) survey with a 250 MHz shielded antenna was conducted along the open-pit edges (Fig. 6), so that the acquired radargrams could be correlated with sedimentological observations from outcrop walls. Flow processing was used to improve the signal-to-noise ratio and correlation of coherent reflection. For this purpose, we applied a static correction of the first arrival, removal of background noise and all very low-frequency components (dewow), automatic and manual signal gain, bandpass frequency filter and a xy-averaging of some traces. Finally, the time-to-depth conversion was performed using velocity determination by a hyperbolic function-fitting for any section containing diffraction or reflection hyperbola.

Depth-converted GPR sections spaced 0.5 m apart were utilized to construct pseudo-3D images using a sequential Gaussian simulation algorithm. The best-fit variogram model showed significant amplitude anisotropy in the NE–SW direction, apparently related to the strike of inclined sand stratification (Fig. 6). The final pseudo-3D GPR cube was constructed as an arithmetical mean (E-type) of 15 equi-probable stochastic realizations of the SGSim algorithm (Kelkar and Perez, 2002). Application of pseudo-3D GPR gives incomplete imaging and limited ability in interpreting sedimentary and tectonic structures, as the acquisition of data is conducted along lines (Christie et al., 2009). To enhance the continuity of stratification and identify major GPR reflectors (e.g., facies contacts), the thin bed indicator attribute was computed as a difference between the weighted mean frequency and the instantaneous frequency (Taner, 1992). Interpretation of synsedimentary faults zones was conducted trace-by-trace, looking for vertical discontinu-

ities in signal amplitude. Semiautomatic extraction and enhancement of faults was supported by computing additional geometrical attributes such as dip variations, similarity and semblance (Taner, 1992).

Palaeocurrent measurements were based on the axes of trough cross-strata sets and the dip direction of planar cross-stratification, and were visualized (Fig. 6) using *EZ-ROSE* software (Baas, 2000). Field measurements were compared and supplemented with the dip azimuths of giant foreset stratification (facies SFi) computed from GPR interfaces (Fig. 7).

3D GEOLOGICAL MODELLING

Systematic documentation and exploration of deposits during the mining operations in Nowodwór-Piaski open pit resulted in a comprehensive dataset of photographs, detailed sketches of outcrop walls and observations on sedimentary structures. The data were georeferenced using local reference grid and then restored to original position during GPS surveys. This database was supplemented and updated with the GPR imagery.

Geomodelling tools were utilized to create a 3D structural model of the normal fault system in one of the study sub-areas (Fig. 5). The *Paradigm GOCAD/SKUA* software was used for surface-based modelling (Caumon et al., 2009) and geostatistical analysis. The software was earlier successfully applied to reconstruct geometrically-complex structural frameworks (Mallet, 1997; Caumon et al., 2009) and depositional architecture of sedimentary basin (Mallet, 2004).

MULTIPLE-POINT STATISTICS

Multiple-point statistics (MPS) algorithms (SNESIM, FILTERSIM, IMPALA, Direct Sampling) are designed to model the spatial relationships and complex architectures of elements

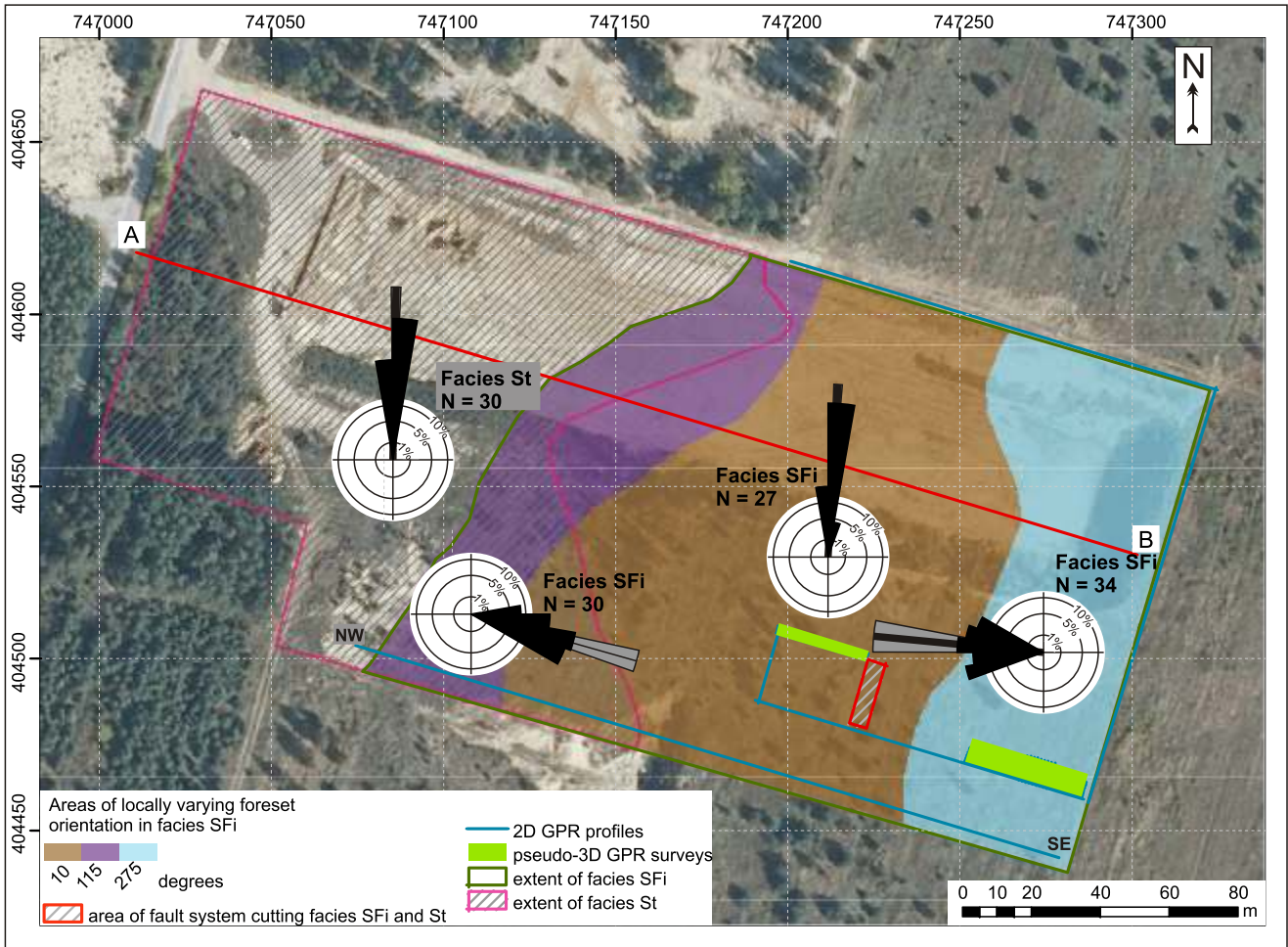


Fig. 6. Facies map of the detailed study area in Nowodwór-Piaski open-pit mine (see red frame in Fig. 1C), showing spatial changes in the direction of inclined stratification in facies SFi documented by measurements in the course of progressive mining

Note the lines of 2D and pseudo-3D GPR sections;
line A–B indicates the geological cross-section with GPR profile shown in Figure 11 and interpreted in Figure 12

such as lithotypes, sedimentary facies or mineral ore structures (Liu et al., 2005; Boucher, 2011). The algorithms combine deterministic aspects of a physical model with its statistical variability (Strebelle and Zhang, 2005). Deployment of a user-defined training image renders this approach unique in comparison to the widely used Monte Carlo variogram-based algorithms. Classical discrete-variable modelling algorithms, such as the *Truncated Gaussian Simulation* or *Sequential Indicator Simulation*, are based on variogram, with the probability density of individual lithotype occurrence obtained by the kriging method (Kelkar and Perez, 2002). However, variogram as a two-point statistic provides only the general maximum and minimum directions of autocorrelation (Gringarten and Deutsch, 2001), while failing to capture local anisotropy of the investigated variable. An MPS algorithm at first stage is scanning the training image and recording for each visited cell its lithotype and the lithotypes present in the neighbouring cells. This approach allows determining of the probability of

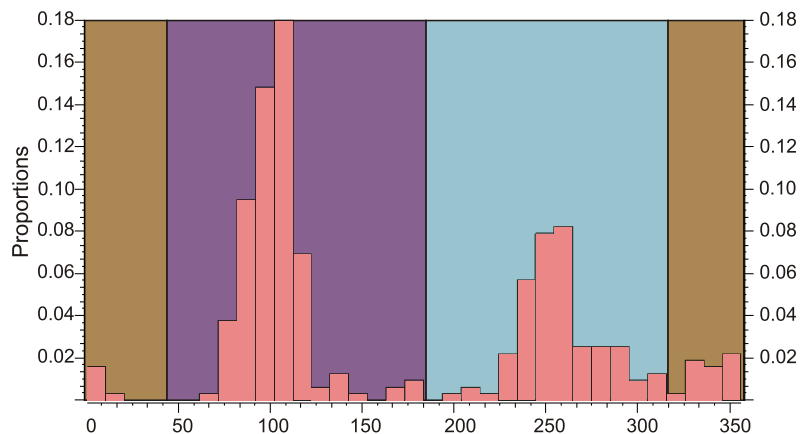


Fig. 7. Histogram of the dip azimuths of giant foreset stratification (facies SFi) derived from GPR data and outcrop measurements

The histogram background colours correspond to those of the map three sub-areas in Figure 6

lithotype occurrence in a given cell relative to the lithotype contents of its neighbours. MPS algorithms are widely used in petroleum reservoir geo-modelling to account for local-scale anisotropies and give ground for detailed fluid-flow simulations (Zappa et al., 2006; Howell et al., 2008).

RESULTS OF THE STUDY

REGIONAL SEQUENCE-STRATIGRAPHIC INTERPRETATION

Regional sequence-stratigraphic analysis was used to establish the palaeogeographic context of environmental changes for the deposition of quartz-glaucconite sands in the study area. As the first step of the spatial stratigraphic analysis, a digital 3D stratigraphic model of the study area was constructed to account for the present-day surface topography, bedrock palaeotopography and the distribution of main sedimentary units on the basis of boreholes and detailed geological maps (Fig. 5). Local-scale VLPDs were constructed to recognize the stratigraphic pattern of lithotype distribution. Lateral nonstationarity of lithotype proportion was examined by separating the borehole data into three zones parallel to the basin's hypothetical southern palaeoshoreline (Kosmowska-Cerano-wicz et al., 1990). The correlation and sequence-stratigraphic synthesis of VLPDs (Fig. 3) revealed a southward expansion of marine sedimentation over a southwards-rising bedrock topography, which justified the geometrical notion of a chrono-stratigraphic onlap for the depositional architecture S as is generally typical of transgressive shallow-marine clastic systems (Posamentier and Allen, 1999; Catuneanu, 2006). It was not obvious which reference level is the most appropriate for the correlation, because of the effects of subsidence and possible syndepositional faulting, a relatively low precision of stratigraphic data and the lack of seismic data for spatial geometry of systems tracts. Therefore, several scenarios of reference level were tested in order to account for uncertainty. A base-lap layering pattern was rejected in favour of an onlap pattern, as the results of the former were fuzzy and not matching the stratigraphic development recognized in the Nowodwór-Piaski pit.

The synthetic VLPD (Fig. 3) shows a sequential development of transgressive and highstand systems tracts spanning six 3rd-order global sea level cycles (Fig. 4; Haq et al., 1987). The sedimentary succession in the study area is interpreted to have commenced with a lowstand systems tract (LST) followed by a marine flooding and a set of three TST-HST sequences of type 2 (Jervey, 1988) masquerading as parasequences. The marine flooding events can be correlated with the transgressive lags (Fig. 3E) cropping out in Siemie near Parczew (Kosmowska-Cerano-wicz et al., 1990). The most conspicuous feature in the VLPD is the abrupt increase of sand proportion directly above the fourth sequence (Fig. 3), which indicates a forced regression corresponding to the Eocene-Oligocene boundary and correlates with the earliest Rupelian eustatic sea level fall (Fig. 4; Haq et al., 1987). This forced regression, with an abrupt transition from lower-shoreface silts to nearshore sands, is attributed by the authors to a regional tectonic uplift (see also Dobrowolski, 1995) that apparently coincided with the eustatic fall. Our evidence of syndepositional faulting in the study area, discussed farther in the text, supports the notion of tectonic activity along this northern margin of the Lublin Highland S probably in response to the northward migration of the Carpathian foreland peripheral bulge (Golonka et al., 2006).

The study area with its north-tilted bedrock (Fig. 2) was a back-bulge depositional zone (*sensu* DeCelles and Giles, 1996) on the northern flank of the subaerial forebulge formed by the structural ridge of Holy Cross Mountains (Golonka et al., 2006) and hence was prone to a flexural extensional deformations (Dobrowolski, 1995).

The depositional forced regression with its lowstand systems tract (FRST and LST in Fig. 4) brought in the main volume of quartz-glaucconite sand to the study area within a relatively short period of time. The sand facies are described and interpreted in detail in the next section. This fifth sequence was of the classical type 1 (Jervey, 1988) and its depositional forced-regressive and lowstand systems tracts are documented here in detail from the Nowodwór-Piaski sand pit near Lubartów. The sixth sequence (Figs. 3 and 4), considered to be of type 2 (Jervey, 1988), is recognizable in boreholes to the south, but is lacking in the study area, where the sedimentary succession was erosionally truncated the Pleistocene ice-sheet before being covered with glacio-fluvial deposits (Fig. 3F).

SEDIMENTARY FACIES

Five main sedimentary facies have been distinguished in the outcrop sections of the Nowodwór-Piaski sand pit on the basis of grain size, stratification type and other macroscopic characteristics. The facies are labelled with the letter code of Miall (1977, 1985), modified by Zieli ski (1995) and Zieli ski and Piekarska-Jamro y (2012), and are summarized in Table 1. They are described and interpreted in more details below.

Facies Sm: structureless coarse-grained sand. This facies is only locally exposed at the bottom of the Nowodwór-Piaski pit (Fig. 8, bottom), but has a thickness of 7–10 m in adjacent boreholes (Kasi ski et al., 1997). It consists of quartz-glaucconite sand with an intense green colour and mainly massive internal structure, but with locally recognizable indistinct traces of planar parallel stratification and asymmetrical wave-ripple cross-lamination accentuated by secondary iron-hydroxide precipitates (Fig. 8, lower left). This facies appears to underlie the graben-fill facies SFi/SFm and locally St in the hanging wall and facies St in the footwall. The sand is markedly coarser-grained than the underlying glauconitic sandy silt and apparently predates shortly the formation of the intra-littoral graben. The lack of mud interlayers and burrows and the occurrence of diffuse relics of wave-formed sedimentary structures support the notion of deposition above the fair-weather wave base (Clifton, 1976; Walker and Plint, 1992). This facies is thought to have been deposited by waves as the forced-regressive systems tract of the fifth stratigraphic sequence (FRST in Figs. 3 and 4), when an upper shoreface zone abruptly shifted northwards into the study area. The homogenized structure of sand can be attributed to seafloor liquefaction caused by the shearing action of seismic ground-roll waves triggered by bedrock faulting (Al-Eqabi and Herrmann, 1993; Al-Shukri et al., 2006).

Facies SFi: sand with giant foreset stratification. This facies (Fig. 8) consists of medium-grained quartz-glaucconitic sand with silty sand interlayers and is volumetrically most important in the Nowodwór-Piaski pit area (Fig. 6). The amount of glauconite grains is relatively low, limited mainly to sediment fraction finer than 0.063 mm. Facies SFi forms two giant (≥ 7 -m-thick) foresets with a high-angle ($>25^\circ$) inclination of strata and dip directions opposing each other. One set is dipping towards the WNW and the other towards the ESE, with a northward dip in their central merger zone (Figs. 6 and 7). The stratification is marked by

Table 1

Main descriptive characteristics and brief interpretation of the sedimentary facies distinguished in the Nowodwór-Piaski sand pit (for details, see text)

Facies code	Textural characteristics	Sedimentary structure	Depositional process	Relationship to rifting
Sm	coarse- to medium-grained glauconite-rich sand; underlain by silty deposits	massive, with diffuse relics of asymmetrical wave-ripple cross-lamination; thickness 7–10 m	upper shoreface deposits formed during a forced regression, probably homogenized by ground-roll triggered by seismic faulting	pre-rift deposits
SFi	medium- to coarse-grained sand intercalated with silty sand	giant-scale high-angle foreset stratification (set thickness 7 m)	fault scarp-attached bar formed by the avalanching of littoral sand supplied by waves, perhaps mainly during storms; some evidence of tidal reworking	syn-rift deposits
SFm	silty sand	massive; multiple subhorizontal beds 10–30-cm-thick, often inversely graded	toeset/bottomset grain-flow deposits related to the foreset facies SFi and attributed to gravitational collapses of upper foreset slope	syn-rift deposits
St	medium-grained sand	trough cross-stratification (set thicknesses 0.10–1.5 m)	migration of subaqueous 3D dunes driven by tidal and wave-generated littoral currents	late syn-rift to post-rift deposits
GSp	gravelly sand and sandy gravel	planar cross-stratification (commonly disturbed by Pleistocene glaciectonic deformation); ~1-m-thick	foreshore deposits formed during a normal marine regression and capping the sedimentary succession; erosionally covered by Pleistocene glacial deposits	post-rift deposits

changes in grain size and occurrence of silty mud drapes, with cross-strata thickness ranging from 0.5 to 10 cm. The foreset layers are mainly massive, but some show heterolithic flaser bedding. The bottomset terminations of cross-strata are often rich in fine gravel and range from angular to tangential, as expected for sediment avalanches (Collinson and Thompson, 1982). GPR sections (shown and discussed farther in the text) indicate that the two large foresets prograded towards each other from syn-sedimentary fault escarpments of a tectonic graben structure ~200 m wide (Fig. 6). They are interpreted to be scarp-attached littoral sand bars whose avalanching slip faces were supplied with sediment mainly by storm waves and modified by fair-weather tidal processes. Comparable features, referred to as intra-shelf accumulation terraces, were described by Jerzykiewicz and Wojewoda (1986), Wojewoda (1986, 1997, 2003) and Łapta (1992).

Facies SFm: structureless fine-grained sand. This facies consists of silty quartz-glauconite sand forming lenticular to wedge-shaped beds with an average thickness of 20 cm, massive internal structure and common evidence of inverse grading (Fig. 8, lower left). The deposits form a subhorizontal bottomset to the foreset facies SFi and are best developed in the central zone of the foreset merger and northward progradation (Fig. 6). At the foreset toe, they form mounded beds or bed packages a few decimetres thick. The origin of this facies is attributed to gravitational, relatively low-friction cohesionless sand flows (grain flows *sensu* Bagnold, 1956; Lowe, 1982) that descended the steep foreset slope and either “froze” at its toe or spread further up to a few tens of metres – forming the subhorizontal bottomset within the graben. The flows were probably triggered by gravitational collapses of the foreset upper slope, as the formation of grain flows requires slope inclination of >25° (Lowe, 1976).

Facies St: sand with trough cross-stratification. This facies (Fig. 8) consists of medium- to coarse-grained quartz-glauconite sand with trough cross-stratification and is thickest (several metres) in the axial part of the graben-fill, while extending laterally beyond the graben margins (see GPR sections in Figure 8 and farther in the text). It overlies erosionally both the

basal facies Sm and the graben-fill facies SFi/SFm towards the north (see the three lower outcrop photographs in Figure 8). The trough cross-strata sets are 0.1–1.5-m-thick and thickening upwards, showing northward transport direction within the graben, but a wider dispersal outside the graben. Some of the trough cross-sets include mud interlayers or mud mixed with fine gravel. Facies St had clearly buried the graben by filling in its axial part and overstepping its margins. This facies represents migration of subaqueous 3D dunes, which are thought to have been driven by prevalent tidal currents within the graben confinement and by wave-generated littoral currents after the graben’s burial (see Clifton et al., 1971; Clifton, 1976; Clifton and Dingler, 1984).

Facies GSp: gravelly sand. This facies consists of planar cross-stratified, medium- to very coarse-grained sand rich in rounded pebbles of quartz and chert up to 2 cm in size (see GSp in Fig. 8). It overlies facies St and locally SFi (see below) with an uneven erosional contact and occurs at the top of the studied succession, where it is sparsely preserved beneath the Pleistocene erosional cover (Fig. 3F). The cross-stratification tends to be disturbed by glacial deformation and obscured by surficial weathering, but seems to be generally dipping towards the north or north-east, away from the southern hinterland. This observation contradicts the previous interpretation of this uppermost facies unit by Morawski (1960) as a transgressive lag (cf. Hwang and Heller, 2002; Cattaneo and Steel, 2003). Instead, this relic unit is thought to represent normal-regressive progradation of foreshore zone that culminated the lowstand systems tract of the last, fifth depositional sequence in the basin (Fig. 4). The uneven erosional base probably reflects shoreline build-out under a varying impact of fair-weather waves and storm breakers.

PALAEOCURRENT ANALYSIS

Palaeocurrent measurements are a crucial part of the present study, as no such analysis was previously conducted in this part of the Polish Lowland Cenozoic Basin. Special attention

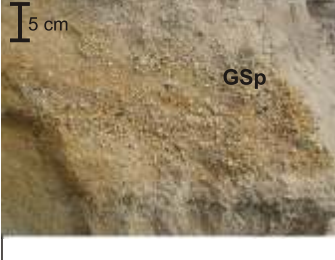
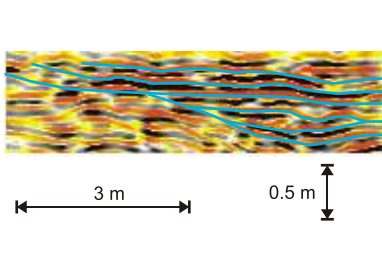
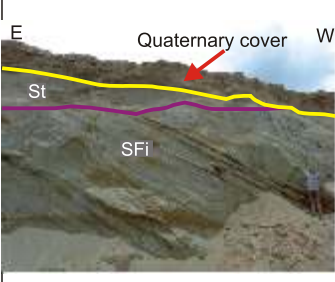
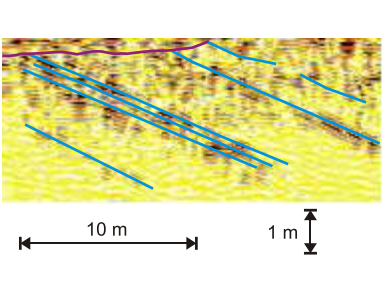
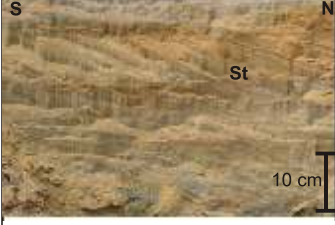
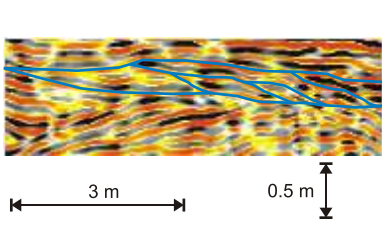
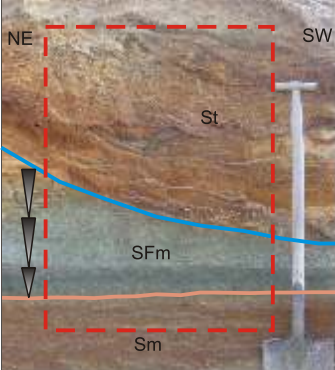
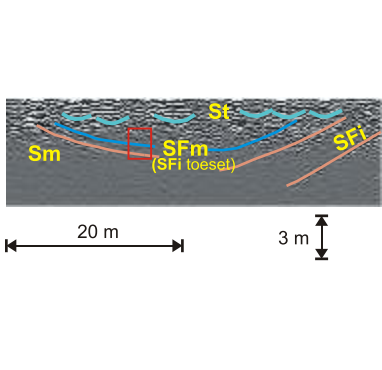
Facies architecture in outcrop section	Facies characteristics	2D GPR pattern perpendicular to palaeocurrent direction
	<p>Facies GSp</p> <ul style="list-style-type: none"> • Poorly sorted sandy gravel • Planar cross-bedding, locally disturbed • Mainly sharp/erosional lower boundary • Transport direction towards the north-east • Occurs locally at the topmost part of the outcrop and overlies large-scale sandy foreset of facies SFi (see Fig. 3F) 	
	<p>Facies SFi</p> <ul style="list-style-type: none"> • Well-sorted, medium-grained quartz-glaucanite sand, with common ripple cross-lamination and silt – draped flaser bedding • Forms two coeval large-scale foresets with opposing directions of bedding dip (towards the WNW and ESE) • Bedding inclination of 20–30° 	
	<p>Facies St</p> <ul style="list-style-type: none"> • Well-sorted quartz-glaucanite sand, medium- to coarse-grained • Forms trough cross-strata sets 0.1–1.5-m-thick • Transport direction towards the north • Overlies erosionally facies SFi and SFm (see below) 	
	<p>Facies SFm</p> <ul style="list-style-type: none"> • Well-sorted quartz-glaucanite silty sand • Forms interbeds, 10–30-cm-thick, at the toe of facies SFi foreset • Subhorizontal or gently inclined in the same direction as the associated foreset beds of facies SFi • Inverse grading <p>Facies Sm</p> <ul style="list-style-type: none"> • Moderately sorted, medium- to coarse-grained quartz-glaucanite sand • Mostly massive structure • Asymmetrical ripples prevail only in the topmost part of profile 	

Fig. 8. Main sedimentary facies distinguished in the Nowodwór-Piaski sand pit and their GPR images

has been given to the dip direction of the high-angle giant foreset stratification of facies SFi, using both outcrop measurements and GPR images (Fig. 9A). The occurrence of this unusual facies in littoral zone and the varied directions of foreset progradation (Figs. 6 and 7) reveal its deposition as the infill of a tectonic graben trending SW–NE, obliquely to the inferred southern palaeoshoreline. GPR images (discussed in the next section) support this interpretation, showing the foresets abutting against fault escarpments (Fig. 9B). The graben-filling foresets apparently prograded towards each other and eventually merged in the southern part of the graben, where the littoral sand supply from shoreline was higher, which resulted in a north-prograding foreset along the graben axis (Fig. 6). This spatial pattern of sedimentation was imposed by the formation of the graben and, apart from the foreset merger in the south and subsequent northward progradation, relates poorly the basin's general palaeogeography.

The regional palaeogeography is reflected better by the trough cross-strata sets of facies St (Fig. 10), which indicate a general northward transport direction of sand (Fig. 6). This spatial pattern can be attributed to storm-generated littoral currents (Walker and Plint, 1992), probably combined with tidal ebb currents within the topographic confinement of the graben. Overall, the palaeocurrent analysis supports the earlier hypothetical inferences of a southern palaeoshoreline in this part of the Paleogene basin (Kosmowska-Ceranowicz et al., 1990; Kasiński and Tolkanowicz, 1999).

RECONSTRUCTION OF 3D SEDIMENTARY ARCHITECTURE

The workflow of multiple-point statistical modelling (Liu et al., 2005) begins with a reconstruction of the structural charac-

teristics of facies and their vertical and lateral organization to create basic training images. These reference 3D models of sedimentary structures serve to represent the elementary architecture of sediment strata, marked by textural grain-size changes and reflecting particular depositional bed forms. The structural models are based on data gathered during fieldwork, such as dimensional drawings of sedimentary structures, sketches of facies architecture observed in outcrop walls and palaeocurrent direction measurements. The progressive mining in the Nowodwór-Piaski pit allowed also recognition of synsedimentary faults and fractures and measuring their spatial orientation (Fig. 9). All these data were used to develop a bulk MPS model of the studied sedimentary succession and to constrain its stochastic realizations.

The 3D modelling at macro-scale pertained to the architecture of strata in the observed range of basic stratification types (Fig. 8), with the construction of training images of particular strata sets or cosets (Figs. 9A and 10). Pseudo-3D GPR images were used to constrain the images. The training images were constructed for the volumetrically dominant facies SFi and St, whereas facies Sm was assumed for simplicity to be homogeneous. The subsequent 3D modelling at meso-scale pertained to the spatial organization of facies (stratification types) and the occurrence of tectonic deformation structures in the sedimentary succession (Figs. 9 and 11). For each area of the occurrence of facies SFi (Fig. 6), the measured mean direction of strata dip was used to rotate appropriately the facies training image of foreset stratification (Fig. 9A) in the MPS bulk 3D

model (Fig. 11, top right). The similar directional procedure was used to create the training image of the trough cross-stratification of facies St (Fig. 10). The spatial relationships of sedimentary facies were constrained by outcrop observations and GPR imagery (Fig. 12).

GPR IMAGING

GPR survey was conducted along the edges of sand pit walls (Fig. 13A), which allowed the images to be directly verified and correlated with outcrop sections (Fig. 13D). Two different sites, with different general direction of foreset dip, were selected for imaging the spatial architecture of facies SFi (Fig. 6). Two parallel 2D GPR sections 0.5 m apart (Fig. 13A) were acquired in order to construct a pseudo-3D GPR cube.

The resolution of GPR images is low (Figs. 12A and 13D), because the sands lack significant gravel interlayers, show gradual and non-systematic textural variation, and also have a reduced and uneven content of capillary water in the neighbourhood of outcrop walls. The contrasts of sediment dielectric properties are thus low, and so is also the depth range of GPR imaging, as the sand transmissibility (propagation velocity) of electromagnetic waves is relatively low (uk, 2011). The best contrast is shown by low-porosity horizons cemented with iron oxides and hydroxides (Fig. 13B), which are parallel to foreset stratification of facies SFi (Fig. 13D). They are a product of the

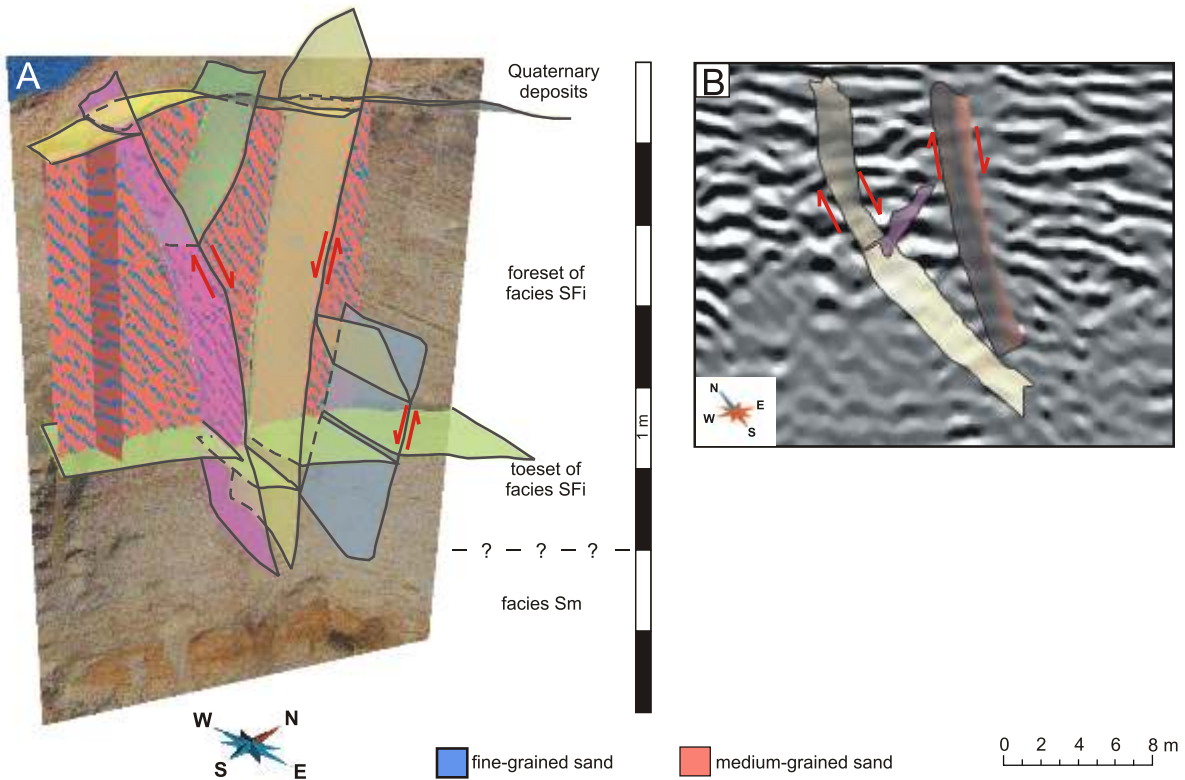


Fig. 9A. 3D model of the foreset of facies SFi with synsedimentary normal faults and fractures; based on GPR imagery combined with multiple-point statistics (numerical impala algorithm); B – GPR image of fault escarpment at the western graben margin

Vertical exaggeration 10x

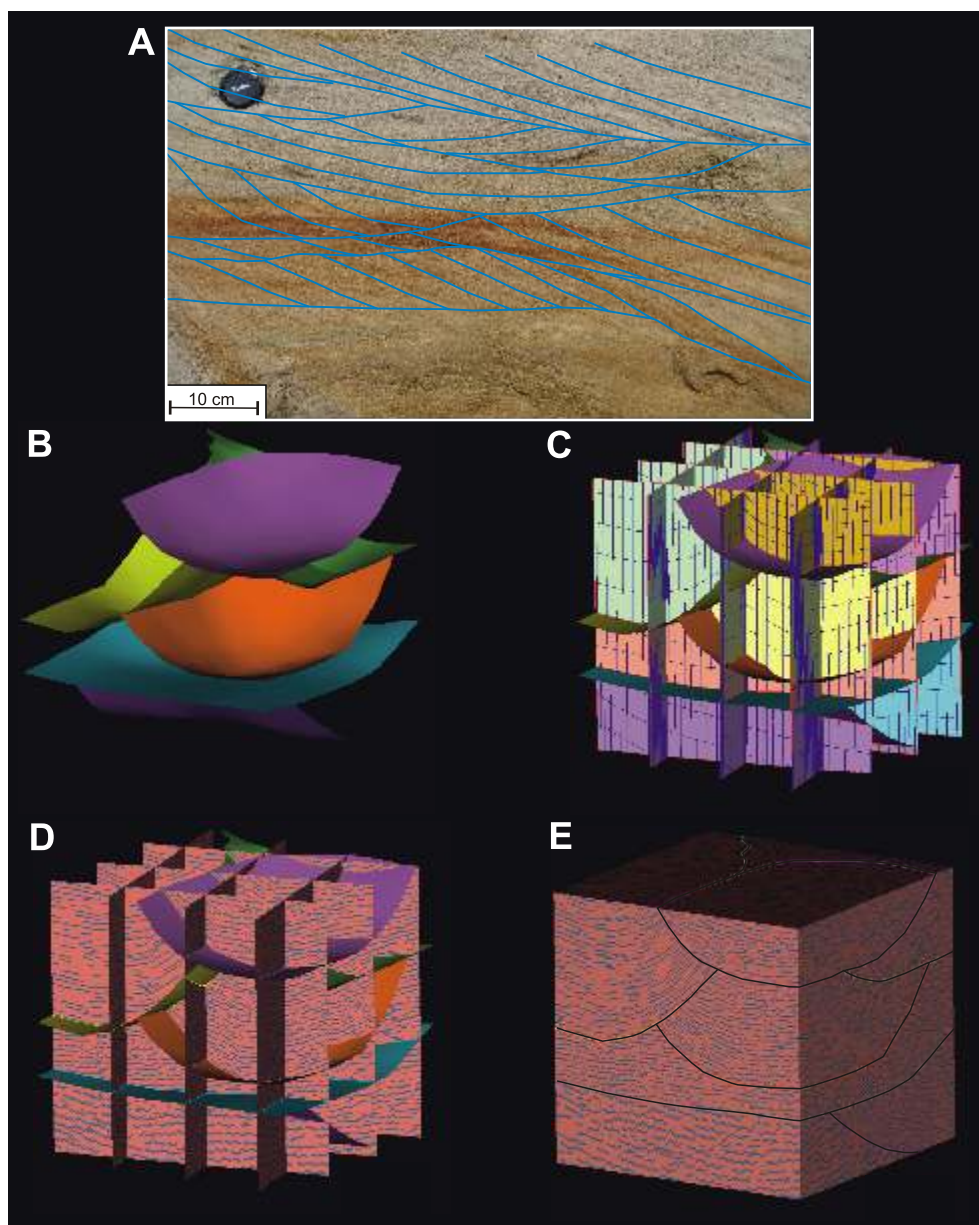


Fig. 10. Construction of a 3D model of sand facies St

A – trough cross-stratified facies St at an outcrop in the Nowodwór-Piaski sand pit; **B** – trough-shaped surfaces are used as a basic structural framework of training image; **C** – 3D image of a spatial grid with stratification parallel to the basal surfaces; **D** – a single modelling realization of the structural heterogeneity of trough cross-stratification; **E** – a cube volume model of facies St as a training image

weathering of glauconite and intra-stratal secondary iron precipitation, related to the groundwater percolation paths along the inclined sand strata (Dam, 2001). Experimental studies by Dam (2001) have shown that although iron oxides as such do not affect directly dielectric properties of sediment, it is the resulting reduction of sediment porosity and permeability and greater content of capillary water that increase the amplitude of refracted electromagnetic wave. Some iron minerals, such as goethite, have also a higher water-retention capacity relative to quartz grains (Dam, 2001).

The occurrence of these iron-cemented markers allowed the foreset stratification of facies SFi to be reliably recognized (Fig. 13D) and its spatial pattern to be modelled (Fig. 13C). The

3D sedimentary architecture of graben-fill deposits was recognized and modelled on this basis, using semblance, entropy and coherency-based techniques. Application of thin-bed indicator has significantly improved vertical resolution and depth extent of radargrams, allowing the graben's boundary faults and related fractures to be recognized (Fig. 12). Nevertheless, the recognition of these synsedimentary faults was difficult, because of the lack of lithological contrast between the footwall and hanging wall and the presence of associated fractures causing scattering of electromagnetic wave. Synsedimentary tectonic deformation is characterized by development of feather-like shear and fracture zones (Wojewoda and Burliga, 2003). The GPR images of fault zones are thus generally fuzzy,

as these zones also tend to be water-saturated, which attenuates electromagnetic signal by decreasing wave amplitude (Prasad et al., 2013).

DISCUSSION OF DEPOSITIONAL SETTING

The study area represents sedimentation at the southeastern outskirts of the Polish Lowland Cenozoic Basin, in the back-bulge zone of the Carpathian foreland peripheral bulge (Fig. 1A). Our sequence-stratigraphic interpretation of the Late Eocene to Early Oligocene sedimentary succession in the study area (Fig. 5) suggests that the end-Priabonian forced regression that brought the main sedimentation phase of quartz-glaucanite sand to the study area was due to a global sea level fall (eustatic cycle TA4.3 of Haq et al., 1987). The regression was probably enhanced by a regional tectonic uplift (Dobrowolski, 1995), as the Carpathian forebulge actively migrated northwards (Wysocka, 1999; Golonka et al., 2006; Oszczytko et al., 2006). The notion of tectonic activity is supported by the syndepositional development of an extensional graben structure in the study area (Fig. 12) and concurs with the earlier suggestion by Kasiński et al. (1997) that the quartz-glaucanite sands in the Lublin region were deposited and preserved under the influence of tectonics.

The tectonic graben documented here had formed across the basin's littoral zone and exerted an important control on the

range of sand facies and their depositional architecture in the study area (Fig. 14). The graben provided intra-littoral accommodation space for the localized accumulation of sand that was derived by storms from the southern shoreline and swept by waves from the graben footwalls. Giant bars attached to the fault escarpments had formed in the graben and eventually merged in its nearshore southern part (diagrams 2 and 3 in Fig. 14). Genetically comparable fault-scarp-attached shallow-marine giant bars are known, for example, from the Miocene on the southern flank of the Carpathian forebulge (Łapta, 1992; Roniewicz and Wysocka, 2001) and from the Intra-Sudetic Cretaceous (Jerzykiewicz and Wojewoda, 1986; Wojewoda, 1986, 1997; Wojewoda et al., 2011). They are distinctly sandy and lack fluvial topsets, and should not be confused with graben-margin Gilbert-type deltas (Colella, 1988; Uliński, 2001; Wojewoda, 2003; Uliński et al., 2009). Importantly, they are intimately related to fault escarpments and hence differ genetically from such features as giant tidal sand-waves (Allen and Homewood, 1984; Green and Smith, 2012), shelf clinoformal deposits (Cattaneo et al., 2007) or prograding coastal spits (Nielsen and Johannessen, 2009; Zecchin et al., 2010). This difference is highlighted by the present case, where the scarp-attached large bars had prograded towards each other within the graben (Figs. 6 and 12), with no obvious adjustment of their geometry to the shoreline. It is only their merger in the southern part of the graben (diagram 3 in Fig. 14) that reflects a greater sand supply and hence proximity to shoreline.

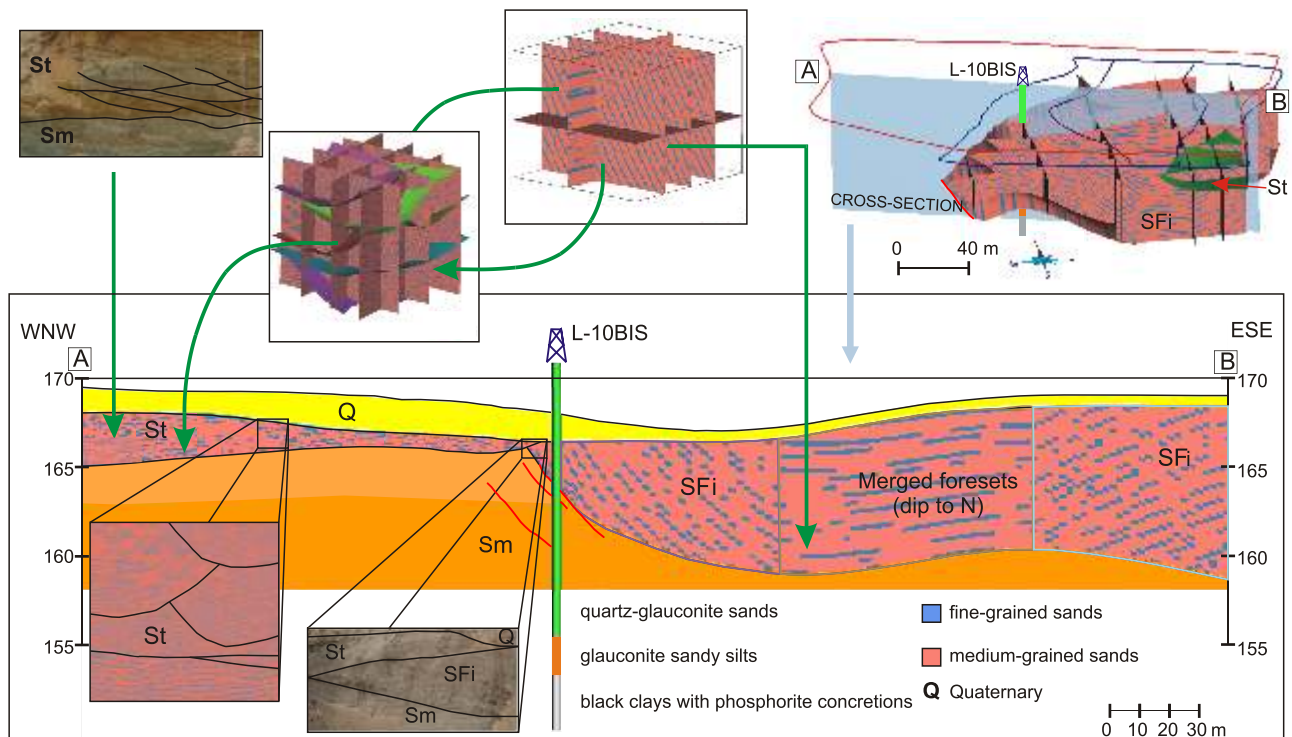


Fig. 11. Reconstruction of the spatial facies relationships and stratification architecture in the study area derived from surface-based modelling and multiple-point statistics

The location of cross-section line ASB is indicated in Figure 6 and the facies code is as used in the text (Table 1); the uppermost part of facies St and the overlying facies GSp are lacking in this cross-section due to Pleistocene erosion; note the reference borehole L-10BIS, located 380 m northwards from the cross-section; the inset images to the left show the stratification anatomy of facies St, whereas the top-right image shows the giant foreset stratification of facies SFi and its transition to facies St at the graben axis

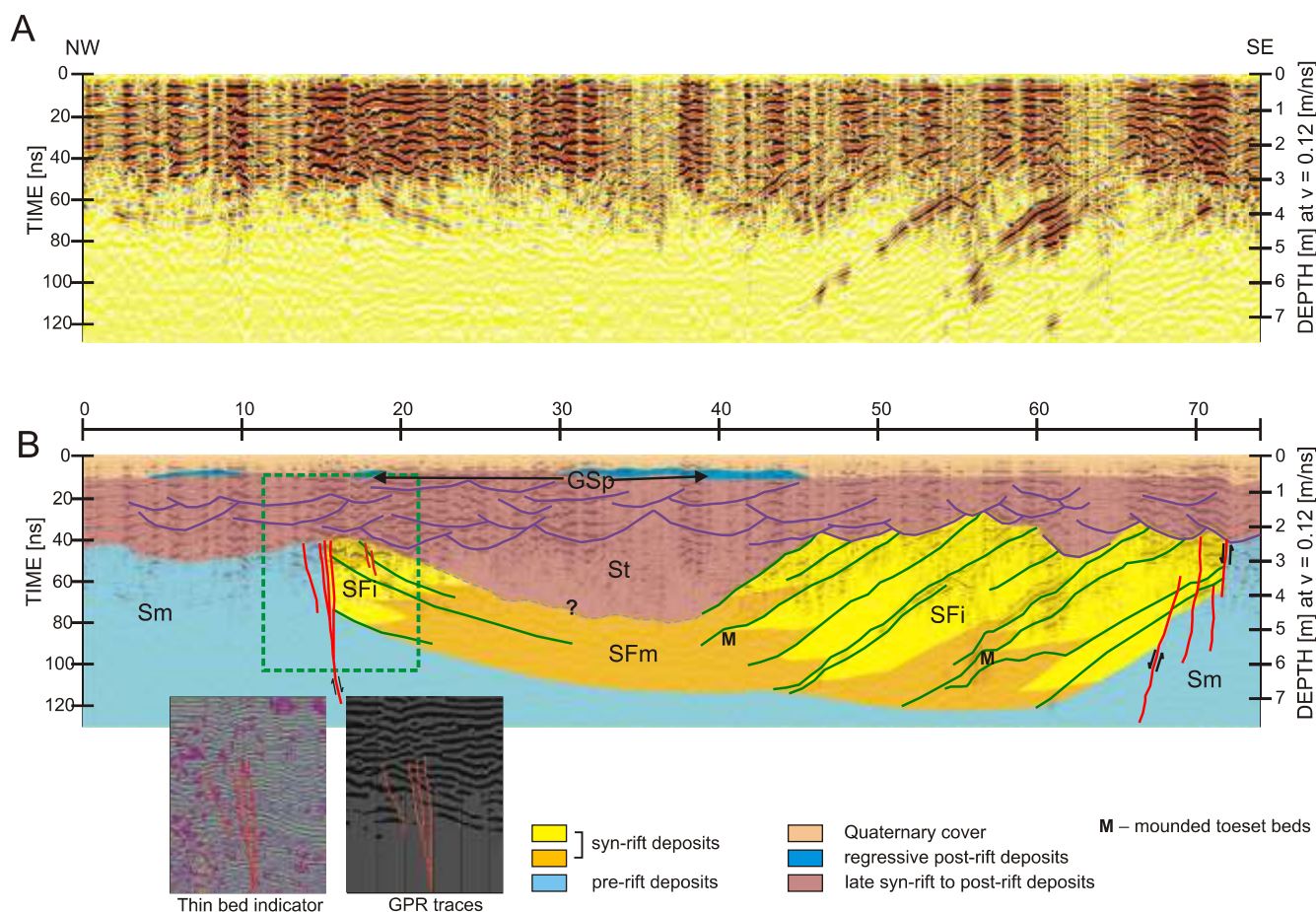


Fig. 12A. 2D GPR section parallel to the sand pit's outcrop wall trending NW–SE (see location in Fig. 4); **B** – interpretation of the GPR section in terms of sedimentary facies architecture, verified by observations from the outcrop wall; the inset images show the GPR signature of synsedimentary faults and related fractures

The topographic confinement of the intra-littoral graben had apparently enhanced the local activity of tidal currents in the depositional forced-regressive systems tract (FRST in Figs. 3 and 4), with the deposition of facies St in the graben driven initially by northward tidal-ebb flow (diagram 3 in Fig. 14). As the subsequent normal regression commenced, the impact of storm-generated seaward rip currents prevailed, while the tectonic activity of the graben gradually declined and its margins became buried by facies St (diagram 4 in Fig. 14). The shoreline had eventually prograded northwards across the study area, leaving an erosional blanket of gravelly facies GSp (diagram 5 in Fig. 14). Deposits of the subsequent last marine transgression and sea level highstand (the uppermost TST and HST in Fig. 3), recognized in wells to the south, are not preserved in the study area, where the Paleogene sedimentary succession was truncated by the regional Pleistocene glacial erosion (see inset C in Fig. 14).

CONCLUSIONS

Sequence-stratigraphic analysis of the Eocene-Oligocene sedimentary succession in the Lubartów area, based on the

VLPD plots of well-log data and verified by evidence from core samples and outcrops, has shed a new light on the palaeogeographic changes at the southeastern outskirts of the Polish Lowland Paleogene Basin. Six sequences have been recognized, correlative with 3rd-order eustatic sea level changes of Haq et al. (1987). The first sequence of type 1 was overlain by three transgressive-regressive sequences of type 2 (*sensu* Jervey, 1988), for which the eustatic fall in relative sea level was compensated by tectonic subsidence. The fifth sequence of type 1 is thought to have been coincided with a regional tectonic uplift (Dobrowolski, 1995), probably related to the northward migration of the Carpathian forebulge. This depositional forced regression and lowstand brought the main volume of quartz-glaucouite sand into the study area. The subsequent sixth sequence of type 2 is recognizable in boreholes to the south, but lacking in the study area, where it was apparently removed by Pleistocene glacial erosion.

Detailed facies analysis of the fifth stratigraphic sequence, exposed in the Nowodwór-Piaski sand pit, has revealed the local spatial pattern of a wave-dominated and tidally-influenced sedimentation, supporting the earlier regional notions of a southern palaeoshoreline (Kosmowska-Ceranowicz et al., 1990; Kasiński and Tołkanowicz, 1999) and a tectonically-controlled sedimentation (Kasiński et al., 1997). The analysis,

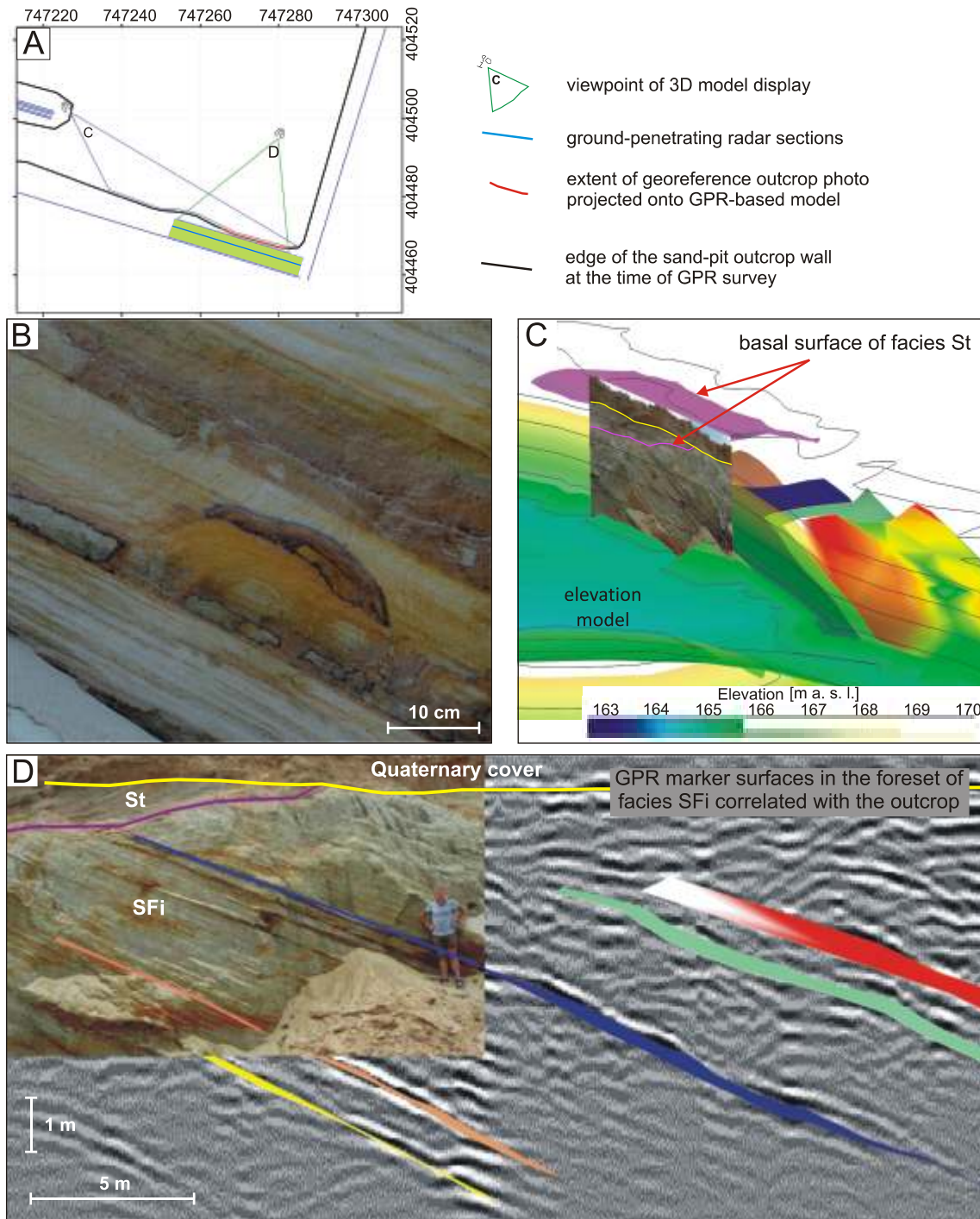


Fig. 13A. Plan-view sketch of the sand-pit mining walls, showing the GPR section lines and the view points for 3D model display; **B** – facies SFi foreset surfaces accentuated by intra-stratal precipitation of iron oxides; **C** – oblique view of the 3D model with inserted outcrop photograph; **D** – orthogonal view of the 3D model, with GPR marker surfaces correlated to the iron oxide-cemented horizons in facies SFi outcrop; the GPR markers represent a significantly lower velocity of electromagnetic wave (Dam, 2001)

aided by multidimensional GPR survey, indicates a syndepositionally-formed tectonic graben filled laterally by fault scarp-attached large sand bars and the axial action of tidal ebb currents. The bars were repositories of shore-derived sand swept by littoral waves, with Miocene analogues on the southern flank of the Carpathian forebulge and Cretaceous analogues in the Sude-

tes. As the graben's tectonic activity ceased, its margins became buried by the lowstand regressive sands. A gravelly shoreline ultimately prograded northwards across the study area, but most of the resulting foreshore deposits were subsequently deformed and removed by the Pleistocene regional glacial erosion.

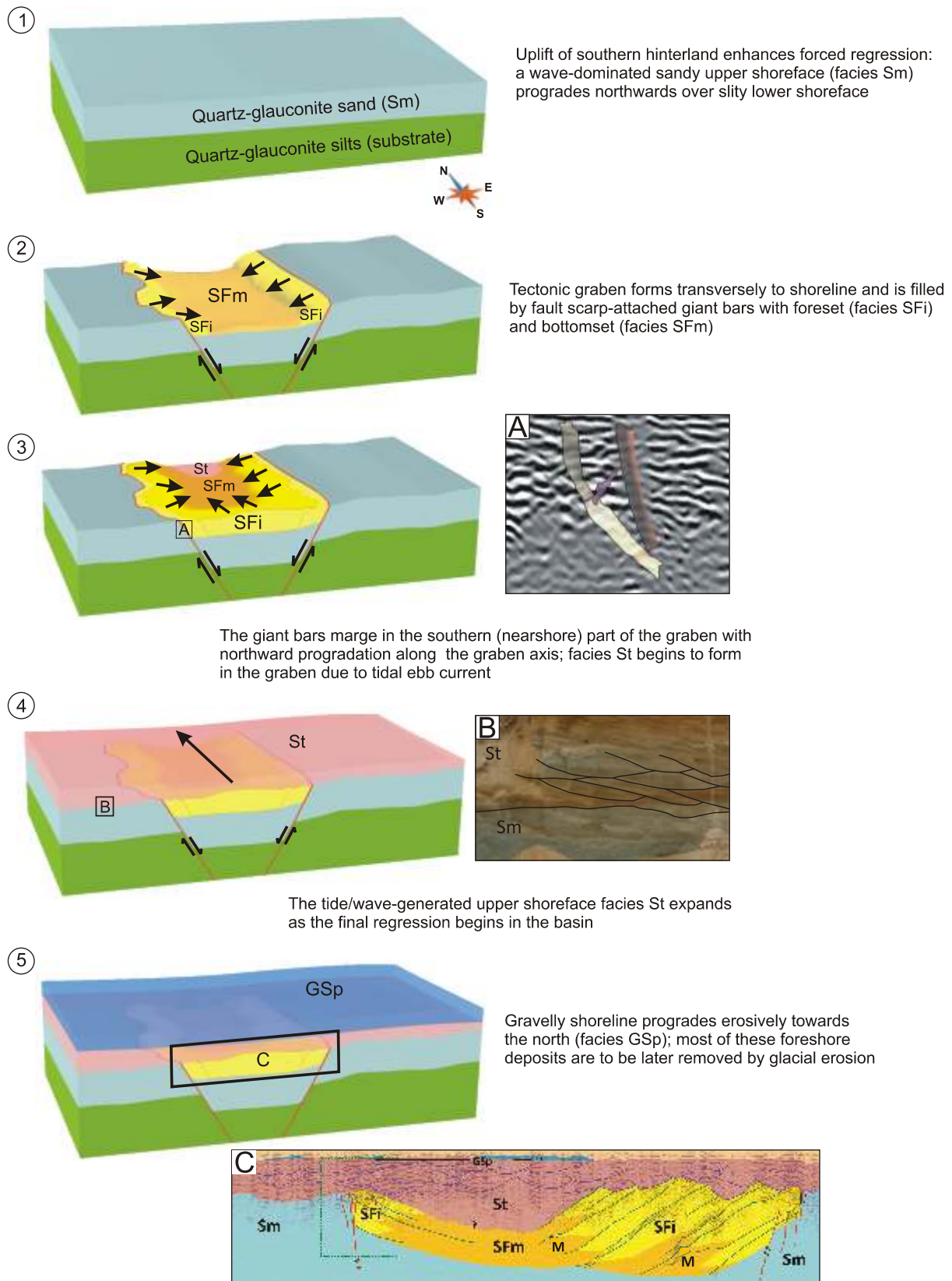


Fig. 14. Cartoon showing a schematic interpretive model for the latest Priabonian-earliest Rupelian sedimentation in the study area near Lubartów, representing the marginal southern part of the Polish Lowland Cenozoic Basin

Vertical scale exaggerated; the graben width is ~200 m and ultimate depth ≤10 m

The 3D model of the fifth-sequence deposits in the Nowo-dwór-Piaski area, constructed with the use of multiple-point statistical methodology, can serve as a guide for the future exploration and exploitation of the quartz-glaucconite sands in the area. It depicts the internal architecture, heterogeneity and spatial relationships of main sedimentary facies and may also serve as instructive example of how the petroleum reservoir

models of complex sedimentary successions can be constructed with the use of modern statistical methods.

Acknowledgements. The manuscript was critically reviewed by W. Nemeč and an anonymous reviewer, whose helpful comments and suggestions are much appreciated by the authors.

REFERENCES

- Aleqabi G., Herrmann R.** (1993) Ground roll: a potential tool for constraining shallow shear-wave structure. *Geophysics*, **58**: 713–719.
- Allen P.A., Homewood P.** (1984) Evolution and mechanics of a Miocene tidal sandwave. *Sedimentology*, **31**: 63–81.
- Al-Shukri H.J., Mahdi H.H., Tuttle M.** (2006) Three-dimensional imaging of earthquake-induced liquefaction features with ground penetrating radar near Marianna, Arkansas. *Seismological Research Letters*, **77**: 505–513.
- Armstrong M., Galli A., Beucher H., Le Loc'h G., Renard D., Doligez B., Eschard R., Geffroy F.** (2011) Plurigaussian Simulations in Geosciences. Springer-Verlag, Berlin.
- Asch K., ed.** (2005) IGME 5000. The 1:5 Million International Geological Map of Europe and Adjacent Areas. BGR, Hannover.
- Baas J.H.** (2000) EZ-ROSE: a computer program for equal-area circular histograms and statistical analysis of two-dimensional vectorial data. *Computers and Geosciences*, **26**: 153–166.
- Bagnold R.A.** (1956) The flow of cohesionless grains in fluids. *Philosophical Transactions of the Royal Society of London*, **A249**: 235–297.
- Buchem F.S.P. van, Doligez B., Eschard R., Lerat O., Grammer G.M., Ravenne Ch.** (2000) Stratigraphic architecture and stochastic reservoir simulation of mixed carbonate/siliciclastic platform (Upper Carboniferous, Paradox Basin, USA). *Bulletin du Centre de Recherches Elf Exploration-Production Mémoire*, **24**: 109–129.
- Boucher A.** (2011) Strategies for Modeling with Multiple-point Simulation Algorithms: Closing the Gap. Gussow Geoscience Conference Proceedings.
- Cattaneo A., Steel R.J.** (2003) Transgressive deposits: a review of their variability. *Earth-Science Reviews*, **62**: 187–228.
- Cattaneo A., Trincardi F., Asioli A., Correggiari A.** (2007) The Western Adriatic shelf clinoform: energy-limited bottomset. *Continental Shelf Research*, **27**: 506–525.
- Catuneanu O.** (2006) Principles of Sequence Stratigraphy. Elsevier, Amsterdam.
- Caumon G., Collon-Drouailler P., Le Carlier de Veslud C., Vieseur S., Sausse J.** (2009) Surface-based 3D modelling of geological structures. *Mathematical Geoscience*, **41**: 927–945.
- Christie M., Tsoxias G.P., Stockli D.F., Black R.** (2009) Assessing fault displacement and off-fault deformation in an extensional tectonic setting using 3-D ground-penetrating radar imaging. *Journal of Applied Geophysics*, **68**: 9–16.
- Clifton H.E.** (1976) Wave-formed sedimentary structures – a conceptual model. *SEPM Special Publication*, **24**: 126–148.
- Clifton H.E., Dingler J.R.** (1984) Wave-formed structures and paleoenvironmental reconstruction. *Marine Geology*, **60**: 165–198.
- Clifton H.E., Hunter R.E., Phillips R.L.** (1971) Depositional structures and processes in the non-barred high-energy nearshore. *Journal of Sedimentary Petrology*, **44**: 651–670.
- Collinson J.D., Thompson D.B.** (1982) Sedimentary Structures. Chapman and Hall, London.
- Colella A.** (1988) Pliocene-Holocene fan deltas and braid deltas in the Crati Basin, southern Italy: a consequence of varying tectonic conditions. In: *Fan Deltas: Sedimentology and Tectonic Settings* (eds. W. Nemeč and R.J. Steel): 50–74. Blackie, London.
- Dam R.L. van** (2001) Causes of Ground-penetrating Radar Reflections in Sediment. PhD thesis, Vrije Universiteit, Amsterdam.
- DeCelles P.G., Giles K.A.** (1996) Foreland basin systems. *Basin Research*, **8**: 105–123.
- Dobrowolski R.** (1995) Mesoscopic tectonic structures in the Upper Cretaceous rocks in the east part of Lublin Upland versus faulting of the East-European Platform basement during the Cenozoic. *Annales Societatis Geologorum Poloniae*, **65**: 79–91.
- Franus M.** (2010) Glaucconite and its geological applications (in Polish with English summary). PhD thesis, Lublin University of Technology, Lublin.
- Franus M., Latosi ska J.** (2009) Wst pna ocena mo liwo ci zastosowania zu ytego zło a glaukonitowego jako surowca do produkcji kruszywa keramzytowego (in Polish). *Budownictwo i Architektura*, **5**: 17–27.
- Franus W., Klinik J., Franus M.** (2004) Mineralogical characteristics and textural properties of acid-activated glauconite. *Mineralogia Polonica*, **35**: 53–60.
- Golonka J., Gahagan L., Krobicki M., Marko F., Oszczytko N., I czka A.** (2006) Plate-tectonic evolution and paleogeography of the circum-Carpathian region. *AAPG Memoir*, **84**: 11–46.
- Green A.N., Smith A.M.** (2012) Can ancient shelf sand ridges be mistaken for Gilbert-type deltas? Examples from the Vryheid Formation, Ecca Group, KwaZulu-Natal, South Africa. *Journal of African Earth Sciences*, **60**: 303–314.
- Gringarten E., Deutsch C.V.** (2001) Teacher's aide: variogram interpretation and modelling. *Mathematical Geology*, **33**: 507–534.
- Haq B.U., Hardenbol J., Vail P.R.** (1987) Chronology of fluctuating sea levels since the Triassic (250 million years ago to present). *Science*, **235**: 1156–1167.
- Helland-Hansen W.** (2009) Towards the standardization of sequence stratigraphy: discussion. *Earth-Science Reviews*, **94**: 95–97.
- Henkiel A.** (1983) Tektonika (in Polish). In: *Symposium: Kenozoik Lubelskiego Zagł bia W glowego*: 41–65. Lublin.
- Howell J., Vassel A., Aune A.** (2008) Modelling of dipping clinoform barriers within deltaic outcrop analogues from Cretaceous Western Interior Basin, USA. *Geological Society Special Publications*, **309**: 99–121.
- Hwang I.G., Heller P.L.** (2002) Anatomy of a transgressive lag: Panther Tongue Sandstone, Star Point Formation, central Utah. *Sedimentology*, **49**: 977–999.
- Jervey M.T.** (1988) Quantitative geological modeling of siliciclastic rock sequences and their seismic expression. *SEPM Special Publication*, **42**: 47–69.
- Jerzykiewicz T., Wojewoda J.** (1986) The Radków and Szczeliniec Sandstones: an example of giant foresets on a tectonically controlled shelf of the Bohemian Cretaceous Basin (Central Europe). *Canadian Society of Petroleum Geologists Memoir*, **11**: 1–15.

- Kasiński J.R., Tołkanowicz E.** (1999) Amber in the northern Lublin region – origin and occurrence. In: Investigations into Amber (eds. B. Kosmowska-Ceranowicz and H. Paner): 41–51. Muzeum Archeologiczne, Gdańsk.
- Kasiński J.R., Tołkanowicz E., Piwocki M., Saternus A., Wojciechowski A.** (1997) Realizacja projektu prac geologicznych dla określenia perspektyw występowania złóż bursztyny w utworach eocenu Lubelszczyzny (in Polish). National Geological Archive, 2529/99, Warsaw.
- Kelkar M., Perez G.** (2002) Applied Geostatistics for Reservoir Characterization. Society of Petroleum Engineers, Richardson, Texas.
- Kosmowska-Ceranowicz B., Leciejewicz K.** (1995) Zło a bursztyny na południowym brzegu morza eocenu. In: II Seminarium Amberif: Znaleziska, zło a i kopalnie bursztyny i innych żywic kopalnych: 32–36. Gdańsk–Warszawa.
- Kosmowska-Ceranowicz B., Kociszewska-Musiał G., Musiał T., Müller C.** (1990) Tertiary amber deposits of Parczew vicinity (in Polish with English summary). *Prace Muzeum Ziemi*, **41**: 21–33.
- Krzowski Z.** (1995) Glaucconite and its geological applications (in Polish with English summary). Wydawnictwo Uczelniane Politechniki Lubelskiej, Lublin.
- Krzywiec P.** (2007) Tectonics of the Lublin area (SE Poland) – new views based on results of seismic data interpretation (in Polish with English summary). *Biuletyn Państwowego Instytutu Geologicznego*, **422**: 5–18.
- Liu Y., Harding A., Gilbert R., Journel A.** (2005) A workflow for multiple-point geostatistical simulation. In: Geostatistics Banff 2004 (eds. O. Leuangthong and C.V. Deutsch), **1**: 245–254. Springer-Verlag, Berlin.
- Lowe D.R.** (1976) Grain flow and grain flow deposits. *Journal of Sedimentary Petrology*, **46**: 188–199.
- Lowe D.R.** (1982) Sediment gravity flows, II. Depositional models with special reference to the deposits of high-density turbidity currents. *Journal of Sedimentary Petrology*, **52**: 279–297.
- Łapta A.** (1992) Giant-scale cross-bedded Miocene biocalcarenes at the northern margin of the Carpathian foredeep. *Annales Societatis Geologorum Poloniae*, **62**: 149–167.
- Łozińska-Stępień H., Rytel A., Saliński P.** (1985) Explanations to Detailed Geological Map of Poland, scale 1:50,000 Lubartów Sheet (in Polish). Polish Geological Institute, Warsaw.
- Mallet J.** (1997) Discrete modelling for natural objects. *Mathematical Geology*, **29**: 199–191.
- Mallet J.** (2004) Space-time mathematical framework for sedimentary geology. *Mathematical Geology*, **36**: 1–32.
- Miall A.D.** (1977) A review of the braided river depositional environment. *Earth-Science Reviews*, **13**: 1–62.
- Miall A.D.** (1985) Architectural element analysis: a new method of facies analysis applied to fluvial deposits. *Earth-Science Reviews*, **22**: 261–308.
- Mojski J.E., Rzechowski J., Woźny E.** (1966) Upper Eocene deposits near Wieprz River in Luszawa (vicinity of Lubartów) (in Polish with English summary). *Przebieg Geologiczny*, **14**: 513–517.
- Morawski J.** (1960) Characteristics of littoral zone sands of lower Oligocene sea of north Lublin region (in Polish with English summary). *Przebieg Geologiczny*, **8**: 628–633.
- Nielsen L.H., Johannessen P.N.** (2009) Facies architecture and depositional processes of the Holocene–Recent accretionary forced regressive Skagen spit system, Denmark. *Sedimentology*, **56**: 935–968.
- Olszewska-Nejbert D., Barski M.** (2007) Uwagi o wieku utworów paleogennych na podstawie cyst *Dinoxagellata* w Mielniku (wschodnia Polska). In: XX Konferencja Naukowa Paleobiologów i Biostratygrafów PTG (w. Katarzyna pod Łysic): 99–100. Polish Geological Society, Kraków.
- Oszczypko N., Krzywiec P., Popadyuk I., Peryt T.** (2006) Carpathian Foredeep Basin (Poland and Ukraine): its sedimentary, structural and geodynamic evolution. *AAPG Memoir*, **84**: 293–350.
- Parecki A., Bujakowska K.** (2004) Dokumentacja geologiczna zło a bursztyny „Górka Lubartowska” w kat. D (in Polish). National Geological Archive, 609/2005, Warsaw.
- Piwocki M.** (2002) Stratigraphy of amber-bearing deposits of northern Lublin region, eastern Poland (in Polish with English summary). *Przebieg Geologiczny*, **50**: 871–874.
- Posamentier H.W., Allen G.P.** (1999) Siliciclastic Sequence Stratigraphy: Concepts and Applications. *SEPM Concepts in Sedimentology and Paleontology*, **7**.
- Prasad P., Ramanujam N., Vignesh A., Murti S.H.K., Rasool Q.A., Biswas S.K., Ojha Ch.** (2013) Ground penetrating radar a tool to map the seismically induced fault and fracture in the coastal cliff of east coast of Port Blair, Andaman. *ARPN Journal of Earth Sciences*, **2**: 9–14.
- Purkis S., Vlaswinkel B., Gracias N.** (2012) Vertical-to-lateral transitions among Cretaceous carbonate facies – a means to 3-D framework construction via Markov analysis. *Journal of Sedimentary Research*, **82**: 232–243.
- Ravenne Ch., Galli A., Doligez B., Beucher H., Eschard R.** (2002) Quantification of facies relationships via proportion curves. In: Geostatistics Rio 2000 (eds. A. Armstrong, C. Bettini, N. Champigny, A. Galli and A. Remacre): 19–39. Springer-Verlag, Berlin.
- Ravenne Ch.** (2002a) Characterization of reservoirs and sequence stratigraphy: quantification and modelling. *Oil and Gas Science and Technology*, **57**: 311–340.
- Ravenne Ch.** (2002b) Sequence stratigraphy evolution since 1970. *Comptes Rendus Palevol*, **1**: 415–438.
- Roniewicz P., Wysocka A.** (2001) Remarks on Miocene sedimentation in the area between Szydłów and Smerdyna, southeastern margin of Holy Cross Mts. (Central Poland) (in Polish with English summary). *Przebieg Geologiczny*, **49**: 639–642.
- Strebelle S., Zhang T.** (2005) Non-stationary multiple-point geostatistical models. In: Geostatistics Banff 2004 (eds. O. Leuangthong and C.V. Deutsch), **1**: 235–244. Springer-Verlag, Berlin.
- Taner M.A.** (1992) Attributes revisited. http://www.rocksolid-images.com/pdf/attrib_revisited.htm
- Tucker M.E.** (2003) *Sedimentary Rocks in the Field*. 3rd Edition, Wiley, Chichester.
- Uberna J., Odrzywolska-Biekowska E.** (1977) New localities of Upper Eocene in northern parts of the Lublin region (in Polish with English summary). *Kwartalnik Geologiczny*, **21** (1): 73–87.
- Uliński D.** (2001) Depositional systems and sequence stratigraphy of coarse-grained deltas in shallow-marine, strike-slip setting: the Bohemian Cretaceous Basin, Czech Republic. *Sedimentology*, **48**: 599–628.
- Uliński D., Laurin J., Kuch S.** (2009) Controls on clastic sequence geometries in a shallow-marine, transtensional basin: the Bohemian Cretaceous Basin, Czech Republic. *Sedimentology*, **56**: 1077–1114.
- Volpi B., Galli A., Ravenne Ch.** (1997) Vertical proportion curves: a qualitative and quantitative tool for reservoir characterization. *Memorias del I Congreso Latinoamericano de Sedimentología. Sociedad Venezolana de Geología*: 351–358.
- Walker R.G., Plint A.G.** (1992) Wave and storm dominated shallow marine system. In: *Facies Models: Response to Sea-Level Change* (eds. R.G. Walker and N.P. James): 219–238. Geological Association of Canada, St. John's.
- Wojewoda J.** (1986) Fault scarp-induced shelf sand bodies: Turonian of the Intrasudetic Basin. In: 7th European Regional Meeting Kraków, Poland. *Excursion Guidebook* (ed. A.K. Teisseyre): 31–52. Publishing House of the Polish Academy of Sciences.

- Wojewoda J.** (1997) Upper Cretaceous littoral-to-shelf succession in the Intrasudetic Basin and Nysa Trough, Sudety Mts. (in Polish). In: *Obszary Źródłowe: Zapis w Osadach* (ed. J. Wojewoda), VI Spotkanie Sedymentologów, **1**: 81–96. Lewin Kłodzki.
- Wojewoda J.** (2003) “Gilbert-type delta” versus “accumulation terraces” models and their application to Middle Turonian–Early Coniacian sedimentary setting in the Intrasudetic Basin: a discussion. *Geolines*, **16**: 110–111.
- Wojewoda J., Burliga S.** (2003) Shear zones in unconsolidated deposits as indicators of synsedimentary tectonic movements. *Geolines*, **16**: 110.
- Wojewoda J., Białek D., Bucha M., Głuszyński A., Gotowała R., Krawczewski J., Schutty B.** (2011) Geology of the Góry Stołowe National Park – selected issues (in Polish with English summary). In: *Geoekologiczne Warunki środowiska Przyrodniczego Parku Narodowego Gór Stołowych* (eds. T. Chodak, C. Kabała, J. Kaszubkiewicz, P. Migo and J. Wojewoda): 53–96. WIND, Wrocław.
- Wołosz E.** (1966a) Eocene deposits from Siemień near Parczew City (in Polish with English summary). *Kwartalnik Geologiczny*, **10** (3): 843–849.
- Wołosz E.** (1966b) Fosforyty i bursztyny z Siemienia koło Parczewa (in Polish). *Przebieg Geologiczny*, **14**: 277–278.
- Wysocka A.** (1999) Depositional and tectonic controls on Early Badenian clastic sedimentation in the Sandomierz–Tarnobrzeg area (Baranów Beds, northern Carpathian Foredeep). *Geological Quarterly*, **43** (4): 383–394.
- Zappa G., Bersezio R., Felletti F., Giudici M.** (2006) Modelling heterogeneity of gravel-sand, braided stream, alluvial aquifers at facies scale. *Journal of Hydrology*, **325**: 134–153.
- Zecchin M., Caffau M., Civile D., Roda C.** (2010) Anatomy of a late Pleistocene clinoformal sedimentary body (Le Castella, Calabria, southern Italy): A case of prograding spit system? *Sedimentary Geology*, **223**: 291–309.
- Zieliński T.** (1995) Kod litofacyjny i litogenetyczny – konstrukcja i zastosowanie osadów czwartorzędowych (eds. E. Mycielska-Dowgiało and J. Rutkowski): 220–235. University of Warsaw, Warsaw.
- Zieliński T., Pisarska-Jamroń M.** (2012) Which features of deposits should be included in a code and which not? (in Polish with English summary). *Przebieg Geologiczny*, **60**: 378–397.
- Zuk T.** (2011) Acquisition, 3-D Display and Interpretation of GPR Data in Fluvial Sedimentology. MSc thesis, University of Birmingham, Birmingham (U.K.).